

Novel Volt/Var Control Strategies for Active Distribution Systems

by

Mehmet Yilmaz

A thesis

presented to the University of Waterloo

in fulfillment of the

thesis requirement for the degree of

Doctor of Philosophy

in

Electrical and Computer Engineering

Waterloo, Ontario, Canada, 2019

© Mehmet Yilmaz 2019

Examining Committee Membership

The following served on the Examining Committee for this thesis. The decision of the Examining Committee is by majority vote.

External Examiner: Hany Farag
Associate Professor, Dept. of EECS, York University

Supervisor(s): Ramadan El-Shatshat
Lecturer, Dept. of ECE, University of Waterloo

Internal Member: Kankar Bhattacharya
Professor, Dept. of ECE, University of Waterloo

Internal Member: Sheshakamal Jarayam
Professor, Dept. of ECE, University of Waterloo

Internal-External Member: Eihab Abdel-Rahman
Professor, Dept. of System Design Eng., University of Waterloo

I hereby declare that I am the sole author of this thesis. This is a true copy of the thesis, including any required final revisions, as accepted by my examiners.

I understand that my thesis may be made electronically available to the public.

Abstract

Power distribution networks are rapidly evolving as active distribution systems, as a result of growing concerns for the environment and the shift towards renewable energy sources (RESs). The introduction of distributed generations can benefit the distribution network in terms of voltage support, loss reduction, equipment capacity release, and greenhouse gas (GHG) emission reduction. However, the integration of RESs into electric grids comes with significant challenges. The produced energy from renewable sources such as wind and solar is intermittent, non-dispatchable and uncertain. The uncertainty in the forecasted renewable energy will consequently impact the operation and control of the power distribution system. The impact on Volt/Var control (VVC) in active distribution systems is of particular concern, mainly because of reverse power flow caused predominantly by RESs. RESs can influence the operation of voltage control devices such as on-load tap changers (OLTCs), line voltage regulators (VRs) and shunt capacitor banks (ShCs). It is mainly because of reverse power flow, caused predominantly by RESs. Reverse power flow or injecting power between the regulator and the regulation point can confuse the local regulator controller, which leads to inappropriate or excessive operations. Some of the potential adverse effects include control interactions, operational conflicts, voltage drop and rise cases at different buses in a network.

This research project aims to carry out an in-depth study on coordinated Volt/Var control strategies in active distribution networks. The thesis focuses on the problem of Volt/Var optimization in active distribution networks, operated under different operating conditions, by taking into consideration the current distribution system requirements and challenges in the presence of high RESs penetration.

In the initial phase of the research project, a generic solution to the VVC problem of

active distribution systems was first developed. The primary goal of this generic solution involved the determination of an optimal control strategy based on system status, which was identified from bus voltages. As such, there are three different operating states; normal, intermediate and emergency state. Each operating state has its own control strategy that includes state-related objective functions, such as minimization of power losses, operational control costs, and voltage deviation. For both normal and intermediate state operations, a heuristic-search based optimization algorithm is implemented. In order to be able to take control actions rapidly, a novel rule-based control strategy is developed for the emergency state.

In the second phase of the research project, the proposed zone-oriented convex distributed VVC algorithm was developed to address the limitations of heuristic optimization algorithms, including long solution times and the non-global optimal solution. The proposed algorithm is based on chordal-relaxation semi-definite programming (SDP), and divides distribution systems into areas based on customer types, wherein, each zone has its own priorities, characteristics, and requirements. The primary goal is to achieve optimal voltage control for each zone, according to its operational requirements and characteristics. Furthermore, in contrast to many decentralized approaches that require iterative solutions to update global multiplier and a penalty parameter to convergence, this method proposes a novel multi-period hierarchical convex distributed control algorithm, requiring no iterative process and no penalty parameter. Eliminating the iterative solution makes convergence fast, while having no penalty parameter allows for the algorithm to be less human and system dependent.

In the final phase of the research project, a 2-stage control algorithm aiming to minimize VR tap movements in convex VVC formulation was developed. In the first stage, the VVC problem is solved for hourly intervals, and VR tap positions are obtained. In the second

stage, control horizon is divided into 15 minutes intervals, and the voltage is controlled only by the RESs' active and reactive power adjustment. The tap movement minimization and 2-stage control algorithm eliminates the excessive use of VRs, prolongs the operational life of VRs and reduces the system operational cost.

The optimal operation of Volt/Var control devices was investigated in the presented Volt/Var optimization methodology. The proposed research will pave the way for managing the increasing penetration of RESs with different types, technologies and operational modes, from a distribution system voltage control perspective. The proposed methodologies in this thesis have been tested on sample distribution systems and their effectiveness is validated.

Acknowledgements

Praise be to Allah, the Creator and Owner of the worlds, whose countless bounties enabled me to accomplish this thesis successfully.

First and foremost, I would like to thank my supervisor Professor Ramadan El-Shatshat for his endless guidance and support throughout my PhD at the University of Waterloo. I also would like to extend my appreciation to my distinguished examining committee members, Professor Kankar Bhattacharya, Professor Sheshakamal Jarayam, Professor Eihab Abdel-Rahman and Professor Hany Farag for their suggestions and corrections that improved the quality of this thesis.

My deepest gratitude and love go to my wife Humeyra Kiyak. I cannot give thanks enough to my beloved wife for her emotional support, understanding and love throughout my PhD journey. She was always with me during my bad and good times. I'm so thankful to Allah for making my life much less of a burden by having Humeyra as a companion. I also would like to thank my family for their support and prayers.

Thanks are also due to the members of my research group, Ayman Othman, Safaon Al-Halali, Monsef Tahir, Jamal Busnaina, and Klaled Elsimisiri for their support and suggestions during the times of struggle.

Finally, I am grateful to my God, Allah (c.c); without Allah (c.c), I could not have achieved all the things that I have today in my life.

Dedication

To my beloved parents, my dear wife Humeyra, and my beautiful daughter Suheyla.

Table of Contents

List of Tables	xv
List of Figures	xvii
List of Symbols	xix
1 Introduction	1
1.1 General	1
1.2 Research Motivations	3
1.3 Research Contributions	4
1.4 Thesis Organization	6
2 Background and Literature Survey	8
2.1 Introduction	8
2.2 Voltage Profile of Passive Distribution Systems	8
2.3 Volt/Var Control (VVC) in Passive Distribution System (PDS)	10

2.3.1	Direct voltage control in PDS	11
2.3.2	Indirect voltage control in PDS	13
2.3.3	Overview of different VVC methods used in PDS	15
2.4	Impacts of RESs on Distribution Systems	16
2.4.1	RES impacts on voltage profile	17
2.5	Volt/Var Control in Active Distribution Systems	18
2.5.1	Local VVC methods in ADSs	19
2.5.2	Coordinated VVC in ADSs	20
2.6	Conclusion	25
3	State-based Volt/Var Control Algorithm for Active Distribution Networks	27
3.1	Introduction	27
3.2	System State Index (SSI)	28
3.2.1	System operating states	29
3.2.2	State switching	30
3.3	Bus Sensitivity Index (BSI)	32
3.3.1	Mathematical model of the BSI	32
3.4	Voltage Sensitivity Analysis	35
3.5	Control Devices	37
3.5.1	Cost Functions of Control Devices	37

3.5.1.1	On-Load Tap-Changer (OLTC)	37
3.5.1.2	Shunt capacitor banks (ShCs)	38
3.5.1.3	Cost of DG active power curtailment	39
3.6	Problem formulation	39
3.6.1	System Objective Functions	40
3.6.1.1	Power loss minimization	40
3.6.1.2	Voltage deviation minimization	40
3.6.2	Device Objective Functions	40
3.6.2.1	Number of tap movement minimization	41
3.6.2.2	DG active power curtailment minimization	41
3.7	Constraints	41
3.7.1	Node power flow constraints	42
3.7.2	Bus voltage limits	42
3.7.3	Capacitor reactive power output limits	42
3.7.4	Transformer tap position constraints	42
3.7.5	DG constraints	43
3.8	Rule-Based Emergency State VVC Algorithm	43
3.9	Optimization Algorithm	44
3.10	Renewable DG and Load Modelling	47
3.10.1	DG Modelling	47

3.10.2	Load Modelling	49
3.11	Case Studies	50
3.11.1	Test Systems	50
3.11.2	Simulation Results	51
3.11.2.1	Base Case Simulation	53
3.11.2.2	State-A simulations	53
3.11.2.3	State-B VVC strategies and simulation	54
3.11.2.4	State-C simulation	55
3.12	Conclusion	56
4	Zone-Oriented Distributed Convex VVC Algorithm	62
4.1	Introduction	62
4.2	System Modelling	62
4.2.1	Renewable Energy Resources (RESs) Modelling	64
4.2.2	Load Modelling	65
4.2.3	Capacitor Bank Modelling	65
4.2.4	Voltage Regulator Modelling	65
4.3	Convex Volt/Var Control Problem Formulation	66
4.3.1	Chordal Relaxation Based VVC Model for Multiphase Radial Distribution Networks	70
4.3.2	Objective Functions	73

4.3.2.1	Minimization of Power Loss	73
4.3.2.2	Minimization of Voltage Deviation	74
4.3.2.3	Minimization of the VR Tap Movement	74
4.4	Hierarchical Distributed Zone-Oriented 2-Stage VVC Strategy	75
4.4.1	System Clustering and Hierarchical Distributed Solution Algorithm	76
4.4.1.1	System Clustering	76
4.4.1.2	Proposed Hierarchical Distributed Solution	79
4.4.2	2-Stage Volt/Var Control Algorithm	80
4.5	Case Studies	81
4.5.1	Base Case (Single Zone, Centralized Solution) Simulation	84
4.5.2	Scenario 1 (3-Zones, Distributed Solution) Simulation	85
4.5.3	Scenario 2 Simulation	86
4.5.4	Scenario 3 Simulation	87
4.5.5	Scenario 4 Simulation	89
4.5.6	Simulations Discussion	92
4.6	Conclusion	94
5	Synopsis and Future Research	95
5.1	Synopsis	95
5.2	Future Work Directions	97
	APPENDIX	99

A Sub-matrix W_s Construction	99
References	101

List of Tables

3.1	Forecasted output power (kW) for Wind DG of a typical day in December	58
3.2	Control Strategies and Corresponding DG Involvements and Objective Types	59
3.3	State A Control Strategies with Corresponding Daily Control Devices States and Objective Function Values for IEEE 34 Bus System	59
3.4	State A Control Strategies with Corresponding Daily Control Devices States and Objective Function Values for IEEE 123 Bus System	60
3.5	State B Control Strategies with Corresponding Control Device States and Objective Function Values	60
3.6	Bus Voltages and BSIs pre- and post-Emergency State Control Actions . .	61
3.7	State C Rule-Based Control Strategy with Corresponding Control Device States and Objective Function Values	61
4.1	Zone-based Control Strategies and Objective Types	76
4.2	Renewable DG Data	82
4.3	Centralized and Distributed Solution Results	84
4.4	Base Case Centralized Solution Daily Power Outputs of Generators	85

4.5	Scenario-2 Hierarchical Distributed Daily Simulation Results	87
4.6	Scenario-3 Hierarchical Distributed Daily Simulation Results ($w_2 = 200$)	89
4.7	Scenario-4 Centralized Daily Simulation Results for Tap Movement	90

List of Figures

2.1	One line feeder and corresponding voltage phasor diagram of a PDS.	9
2.2	Basic OLTC Structure.	12
2.3	A typical voltage regulator control mechanism.	13
2.4	Simple one-line diagram of a feeder with a RES connected to the feeder-end.	18
2.5	Simple one line representation of local VVC.	19
2.6	Simple centralized VVC Schematic.	21
3.1	Illustration of voltage boundaries and ranges specified by ANSI C84.1	29
3.2	System state-switching scheme	31
3.3	Flowchart of the proposed state-based VVC algorithm	33
3.4	One line diagram of a two-bus distribution network.	34
3.5	Flowchart of the proposed rule-based VVC algorithm	45
3.6	Pareto-Front concept of two objective problem solution.	46
3.7	Daily load profiles for different seasons.	50
3.8	One-line diagram of the modified IEEE-34 bus test system.	51

3.9	One-line diagram of the modified IEEE-123 bus test system.	52
3.10	Phase-A daily voltage profile of the Bus 890.	55
4.1	Equivalent circuit of VR transformer	66
4.2	Flowchart of the proposed hierarchical distributed algorithm.	77
4.3	Time resolution of the proposed 2-stage control algorithm.	81
4.4	One-line diagram of the modified IEEE-34 bus test system.	82
4.5	Daily load profiles for different customer types.	83
4.6	Daily VR-1 tap positions in Scenario 3.	88
4.7	Daily VR-2 tap positions in Scenario 3.	88
4.8	Actual and forecasted solar DG's active power output for 15-minutes intervals.	90
4.9	Hourly forecasted solar-based RES active power output.	91
4.10	VR tap positions for single-stage control solution with discrete tap modelling.	91
4.11	VR tap positions for two-stage control solution with discrete tap modelling.	92
4.12	Reactive power injection of each DG for single-stage control with discrete tap modelling.	93
4.13	Reactive power injection of each DG for two-stage control with discrete tap modelling.	93

Nomenclature

Acronyms

ADS	Active distribution system.
DG	Distributed generation.
DSO	Distribution system operator.
EESS	Electrical energy storage system.
LDC	Line-drop compensator.
OLTC	On-load tap changer.
PDS	Passive distribution system.
PT	Potential transformer.
PV	Photovoltaic.
RES	Renewable energy resource.
ShC	Shunt capacitor bank.
SSI	System state index.

VR Voltage regulator.

VVC Volt/Var control.

Constants

η_{DG} Loss factor of inverter.

S_g^{max} Maximum apparent power limits of the inverter for RES g .

$V_{i,t}^{set}$ Voltage reference value at bus i for time t .

w_0, w_1, w_2 Objective function weight coefficients.

Sets

ϵ Set of lines.

\hat{N}_c Set of neighbor areas of area c .

Ω_n Set of buses that are connected to bus n .

ψ_n Set of phases of bus n i.e., $\{a, b, c\}$.

c Set of zones.

C_s Set of shunt capacitors.

DG_n Set of DG connected buses.

K Set of VRs.

N, N_g, N_l Set of system buses, generators and loads.

S Set of sub-matrixes.

Variables

$ \cdot $	Number of element in a set.
$(\cdot) \succeq 0$	Positive semidefinite.
$(\cdot)^H$	Conjugate transpose operator.
$(\cdot)^T$	Transpose operator.
$(\cdot)^{max}$	Upper bound of a certain parameter.
$(\cdot)^{min}$	Lower bound of a certain parameter.
δ_i	Power angle of bus i voltage.
$abs(\cdot)$	Magnitude of a parameter.
C_{DG}^P	Control cost of DG's active power (\$).
C_{OLTC}^R	Cost of replacing the OLTC (\$).
C_e	Contract energy price (¢/kWh).
C_{OLTC}	Cost of tap action for the OLTC transformer (\$).
C_{ShC}^f	Fixed cost of the new capacitor bank (\$).
C_{ShC}^t	Cost of the capacitor reactive power injection for time t (\$).
G_{ij}	Conductance of the line between buses i and j .
$kVAr$	Kilo Volt Ampere reactive.
kW	Kilowatts.
LS_{OLTC}^T	Total lifespan of the OLTC.
LS_{OLTC}^R	Remaining lifespan of the OLTC.

LT_{ShC}	Service life of capacitor.
n	Total number of buses.
N_{OLTC}^R	Remaining OLTC tap operating times.
N_{OLTC}^T	Estimated total OLTC tap operating times.
$P_{curt.}$	Curtailed DG active power.
$P_{DG,t}^f$	Forecasted DG power output at hour t .
$P_{DG,t}^{inj}$	Active power injection of DG at hour t .
$P_{DG_i,t}$	Active power of DG i at time t .
$P_{gi,t}$	Active power generation at bus i at time t .
$P_{li,t}$	Active load demand at bus i at time t .
P_{Loss}^t	Active power loss at hour t .
$Q_{DG_i,t}$	Reactive power of DG i at time t .
$Q_{gi,t}$	Reactive power generation at bus i at time t .
$Q_{li,t}$	Reactive load demand at bus i at time t .
$Q_{ShC,t}$	Reactive power injection at time t .
$Q_{ShC_i,t}$	Reactive power injection from capacitor bank i at time t .
$rank(\cdot)$	Rank of a matrix.
ShC^r	Reactive power generated by the capacitor bank (kVAR).
T	Number of time intervals.

$tr(\cdot)$	Trace operator.
V_i^{max}	Maximum voltage level at bus i .
V_i^{min}	Minimum voltage level at bus i .
V_D	Voltage deviation.
V_{DB}	Deadband voltage.
$V_{i,t}$	Voltage value of bus i at time t .
$V_{i,t}^m$	Measured voltage value for bus i at hour t .
$V_{i,t}^{set}$	Voltage set value at bus i at hour t .
P_{DG}, Q_{DG}	Active/Reactive power of the DG.
P_{ij}	Active power flow from bus i to j .
$P_{n,d}^\phi, Q_{n,d}^\phi$	Active/reactive loads at phase ϕ of bus n .
$P_{n,g}^\phi, Q_{n,g}^\phi$	Active/reactive power generation at phase ϕ of bus n .
P_n^ϕ	Active power injection of phase ϕ from bus n .
PF	Power factor.
Q_n^ϕ	Reactive power injection of phase ϕ from bus n .
$Q_{s,q}^\phi$	Reactive power injection of phase ϕ from capacitor s .
S_n^ϕ	Complex power injection of phase ϕ from bus n .
$T_{n,m}^\phi$	Tap ratio of phase ϕ of VR between bus n and m .
$Tap_{i,t}$	Tap position of i^{th} VR at hour t .

V Vector of complex voltage variables.

V_n^ϕ Complex voltage at phase ϕ of bus n .

Chapter 1

Introduction

1.1 General

Voltage regulation using Volt/Var control (VVC) devices is an important operation within distribution networks. An efficient VVC can improve operational efficiency, minimize electrical losses, as well as improve service quality for better profitability. The primary objective of the VVC is to maintain acceptable voltages at all points along the distribution feeder under all loading conditions, as specified by ANSI standard C84.1-2011 [1]. Traditional Volt/Var control (VVC) practice is to regulate the feeder voltage by adjusting the taps of substation on-load tap changer transformers (OLTCs), switched shunt capacitor banks (ShCs), and voltage regulators (VRs). These Volt/Var control devices are installed on the primary feeder and are controlled by local controllers. Some of these devices use autonomous controllers, typically mounted onto them, which take control decisions based on local voltage and current measurements. Others use line drop compensation (LDC) for automatic control of VRs and/or the OLTCs tap position in order to regulate the voltage

at a point along the feeder.

Furthermore, due to the negative environmental impact of greenhouse gases (GHG), there has been an increased interest in distributed Renewable Energy Sources (RESs). The penetration level of renewable distributed generation (solar and wind) has been expected to increase in the near future. The cumulative capacity of wind turbines installed worldwide reached 564 gigawatts (GW) by the end of 2018, and the generation capacity increased by 49 GW only in 2018, representing almost a 10% growing rate. Similarly, the overall solar power generation capacity reached 486 GW by end of 2018, with a capacity addition of 94 GW in 2018, representing approximately a 24% capacity increase [2].

Unfortunately, RESs cannot fit seamlessly in the conventional power distribution system, which is designed and operated without any distributed generation in mind. The integration of RESs and their associated dynamics into existing distribution networks has changed the way the distribution system is operated, in particular, in relation to the VVC. With the increased penetration of RESs into the distribution system, reliable system operation and control has become increasingly difficult, as the power flow no longer remains unidirectional. The high penetration level of RESs in active distribution systems (i.e., distribution systems with RESs) is also accompanied by challenges, including voltage profile variation due to the random variations in the power outputs, which may push the bus voltages out of the limits set by ANSI standard C84.1-2011. In addition to this, renewable sources may cause reverse power flow at times of high penetration with light loads, which can interfere with local controllers of Volt/Var devices. The reverse power flow or injecting power between the regulator and the regulation point can confuse the local regulator controller, leading to inappropriate or excessive operations. For this reason, the development of an efficient VVC methodology that takes into consideration the challenges facing conventional VVC practices is necessary. As such, this thesis investigates and presents a

new Volt/Var control methodology, while addressing current power system requirements and challenges in the presence of high RES penetration.

1.2 Research Motivations

The incorporation of distributed RESs requires a change in the method by which electric utilities operate. As mentioned above, the VVC is an important operation that can be affected by the implementation of distributed RESs. Weather conditions dictate solar and wind generation units, and as such, this introduces undesired uncertainty to the VVC problem. A significant amount of work has been published on VVC in distribution systems, through the application of a variety of techniques [3–9]. Most of the existing algorithms in literature address the VVC problem for a steady-state operating condition, while the objectives and controllers are usually kept fixed for the entire operation period. This methodology might not be an optimal approach at all times under new power grid operating conditions, due to drastic changes in the fundamentals of the conventional power grid. Furthermore, choosing objectives and control entities arbitrarily for the VVC problem may not yield the best results for different power grid operation states, such as steady-state, intermediate and emergency state. High uncertainty in RESs' power generation creates an extra burden on existing VVC devices, resulting in excessive VR tap movement, along with poor voltage regulation. Therefore, there is a need to develop a new VVC algorithm that takes new power grid concepts into consideration, in which the issue of high RESs penetration creating high uncertainty in distribution network conditions due to their volatile power output is addressed.

Furthermore, voltage regulation problems are generally addressed with centralized control schemes. This involves a master controller that collects the system state information,

processes the collected data, creates a control signal, and sends the signal to different slave entities located along the feeder. This type of approach requires large amounts of data to be transferred between the master controller and slave entities, thus creating high levels of complexity in communication and computation. The aforementioned problems become more severe, especially with a high penetration of RESs in larger power systems, due to increased control variables in the system. The centralized approach is also not favourable due to privacy concerns about consumer data, which is vulnerable to cyber attacks. To challenge this communication and computation complexity in the centralized approach, decentralized (distributed) control approaches have been proposed that require less communication and computation effort.

1.3 Research Contributions

The main objective of this dissertation is to develop effective VVC techniques suitable for active distribution systems that can actively control feeder voltage profiles under different operating conditions (steady-state, intermediate and emergency state). The following are the main contributions to this thesis:

1. Development of a comprehensive state-based VVC algorithm that adjusts the control objectives and controllers according to the power grid status, in orders to ensure effective and optimum control for different grid operating conditions. The developed algorithm enables distribution system operators (DSOs) to identify the best VVC practice for a given system state and constraints, where the state is identified based on distribution system bus voltages.
2. Development of a rule-based VVC algorithm for emergency state operation, which

eliminates computational time barriers and enables DSO to act quickly under emergency circumstances, so as to avoid any service interruption.

3. Development of a distributed convex VVC algorithm that meets specific requirements for different customer classes by formulating a unique VVC problem for each customer type. A novel clustering technique has been developed to divide typical distribution systems into areas based on customer class (residential, commercial and industrial end-users), wherein each class has its own objective(s) and constraints. Furthermore, contrary to most decentralized approaches that require iterative solutions to update global multipliers and penalty parameters to convergence, this method proposes a novel multi-period hierarchical convex distributed control algorithm that requires no iterative process and no penalty parameter. Eliminating the iterative solution makes convergence fast, while having no penalty parameter makes the algorithm less human and system dependent. It is also worth mentioning that the proposed VVC solution technique guarantees the global optimal solution by having a rank-1 decision variable matrix, which is not applicable to non-convex versions of VVC optimization techniques.
4. Development of a 2-stage control algorithm that minimizes VR tap movements, which has not been considered before in convex VVC formulation. The proposed 2-stage VVC algorithm minimizes the negative impact of RESs on VR. In the first-stage, the VVC problem is solved for hourly intervals, and VR tap positions are obtained. In the second-stage, the solution resolution is divided into 15-minutes intervals, and the voltage is controlled by only the RESs' active and reactive power adjustment. The tap movement minimization and 2-stage control algorithm eliminates excessive use of VRs, prolongs the life of VRs and reduces the operational cost.

1.4 Thesis Organization

This thesis contains five chapters. The first chapter is the introductory chapter, presenting a brief general introduction, the research motivations, and the research contributions. The following chapters are organized as follows:

1. Chapter 2: Background on voltage control techniques, followed by a comprehensive literature review of Volt/Var control methods for passive and active distribution systems. This chapter also presents an overview of the distributed generation impact on the voltage profile and VVC algorithms.
2. Chapter 3: In this chapter, we first identify the system state index based on the voltage profile, and present the transaction scheme between states. Next, we formulate the bus stability index to identify the weakest bus in the system, with voltage sensitivity analysis of the buses. Then, we formulate the cost of control devices, objective functions, and constraints, and the proposed rule-based algorithm for the emergency state is presented.

In the simulations section, we first discuss and present the optimization algorithm used in solving the proposed VVC problem with the Pareto optimality are discussed and presented. Next, the forecasting model for wind power generation is discussed with consideration of forecast error. Then, the proposed state-based VVC algorithms are tested on IEEE-34 and IEEE-123 bus radial distribution test systems to verify the effectiveness of the developed algorithm. Finally, different scenarios are simulated and the results are analyzed and presented.

3. Chapter 4: Different system component models are provided, and an overview of positive semi-definite formulation of power flow equations is presented. In addition,

chordal relaxation based formulation of the VVC problem is provided. This is followed by the proposed clustering method and hierarchical distributed zone-oriented convex VVC problem and solution algorithm, and lastly, simulation results and conclusion are presented.

4. Chapter 5: This chapter consists of two parts. It first summarizes a number of key attributes of the thesis, and then highlights potential future work directions.

Chapter 2

Background and Literature Survey

2.1 Introduction

This chapter provides a comprehensive review of Volt/Var control methods for both passive and active distribution systems. It also presents an overview of distributed generation impact on the voltage profile and VVC algorithms.

2.2 Voltage Profile of Passive Distribution Systems

Passive Distribution Systems (PDSs) have unidirectional power flow from the central power supply to the end users along the feeders. In this one-way flow concept, the feeder voltage profile decreases along the feeder, reaching the minimum at the end of the feeder. However, the voltage profile can only vary between certain predefined upper and lower limits, known as ANSI-C84.1 standard; therefore, keeping the voltage within the allowed limits is an

important power quality issue in DSs [10]. The ANSI-C84.1 standard limits according to a 120 V nominal voltage can be summarized as follows:

- Under normal operating conditions (Range A), the regulation requirement is +/-5%.
- Under abnormal conditions (Range B), the regulation requirement is -8.3% to +5.8%.

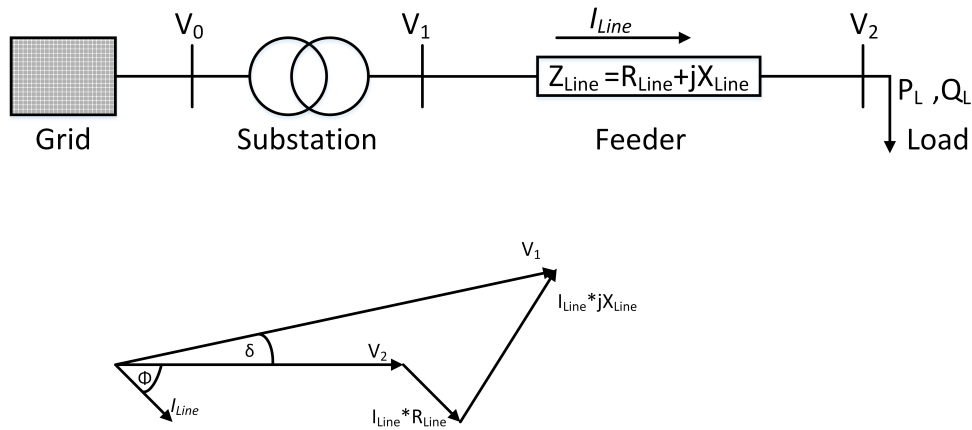


Figure 2.1 One line feeder and corresponding voltage phasor diagram of a PDS.

A one line diagram of a basic PDS and the corresponding voltage phasor are shown in Fig 2.1. The line current I_{Line} is unidirectional from the substation to the load node and can be expressed as follows:

$$I_{Line} = \frac{S^*}{V_2^*} = \frac{P_L - jQ_L}{V_2^*} \quad (2.1)$$

where S , P_L , and Q_L are the complex power, active power and reactive power respectively, and U_2 is the load bus voltage.

The voltage difference between substation and load bus is called voltage drop on the

feeder, and calculated as follows:

$$|V_1 - V_2| = |I_{Line}(R_{Line} + jX_{Line})| = \left| \frac{(R_{Line}P_L + X_{Line}Q_L) - j(X_{Line}P_L - R_{Line}Q_L)}{V_2} \right| \quad (2.2)$$

where R_{Line} is the line resistance and X_{Line} is the line reactance.

The imaginary part of equation (2.2) can be neglected for small power flow due to small voltage angle δ between V_2 and V_1 , and the voltage drop $\Delta V = |V_1 - V_2|$ can be approximated as:

$$\Delta V \approx \frac{(R_{Line}P_L + X_{Line}Q_L)}{V_2} \quad (2.3)$$

It can be driven from equation (2.3) that active and reactive power flows cause voltage drop along the feeder, and that sometimes the drop can violate the minimum allowed voltage limit.

2.3 Volt/Var Control (VVC) in Passive Distribution System (PDS)

Voltage violation is an important issue both in terms of system reliability and customer satisfaction, so DSOs utilize Volt/Var control algorithms to avoid or eliminate the violations. In order to ensure the voltage stays within the limits at all times and all loading conditions, traditional VVC algorithms utilize common control devices which are [11]:

- On-Load Tap Changer Transformers (OLTCs)
- Voltage Regulators (VRs)

- Shunt Capacitor Banks (ShCs)
- Static Var Compensators (SVCs).

Two main methods exist for voltage control; the direct method, which can increase or decrease the voltage by tap movements, and the indirect method, which is mainly utilized for reactive power compensation, but also controls the voltage indirectly.

2.3.1 Direct voltage control in PDS

Voltage control in PDSs is typically done by adjusting substation transformer ratio settings with the load tap-changer (LTC). Transformers with LTC have the ability to adjust tap ratio settings either when the transformer is energized (OLTC), or when it is de-energized (no-load tap-changer). Only OLTCs will be considered in this work, since they have been used commonly in PDSs. A basic OLTC arrangement is shown in Fig 2.2, in which PT is potential transformer and Vset is voltage set point. The LTC can be operated manually or by an automatic voltage control relay (AVR). The OLTC controller keeps the substation transformer secondary side voltage V_1 constant within the range

$$V_{LB} \leq V_1 \leq V_{UB}$$

where

- $V_{LB} = V_{set} - 0.5V_{DB}$ is the lower boundary voltage;
- $V_{UB} = V_{set} + 0.5V_{DB}$ is the upper boundary voltage; and
- V_{set} is the set point voltage and V_{DB} is the dead band.

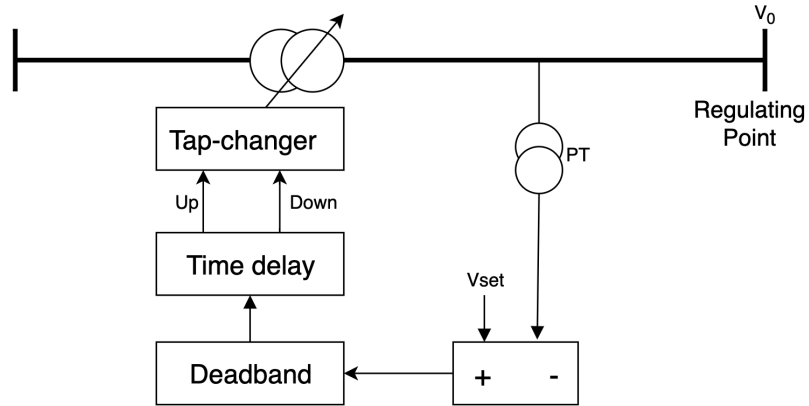


Figure 2.2 Basic OLTC Structure.

The dead band is needed to avoid oscillations and hunting (repeated activation and deactivation cycle) of the tap changer. The time delay element is to avoid tap changer operation in case of short-time voltage variations. Modern automatic voltage relays (AVRs) may obtain a line drop compensation (LDC) feature that allows the controller to regulate voltage at a remote node (called load center/regulating point). The LDC estimates the load center voltage by using user defined LDC impedance settings (R_c and X_c), and measured substation current. The resistive and reactive element in the LDC circuit is set to simulate the resistance and reactance of the line from regulator to the load center.

Another direct control device is the voltage regulator (VR), which consists of an auto-transformer and an LTC mechanism. The voltage changes are obtained by changing the position of the tap that is controlled by the LDC circuit. Standard VRs contain $\pm 10\%$ regulator range, usually with 16 steps up and 16 steps down, which provide 0.75 volts change per step on a 120 volt base. A VR equipped with LDC is shown in Fig. 2.3, and typical operation logic can be explained as follows:

- First, the voltage sensing controller calculates the load center's voltage and compares it with the voltage set value;
- Second, if the difference between calculated and set value is more than one half of bandwidth and remains for the time delay period, then;
- Lastly, the controller sends a command to LTC to lower or raise the tap ratio of the VR.

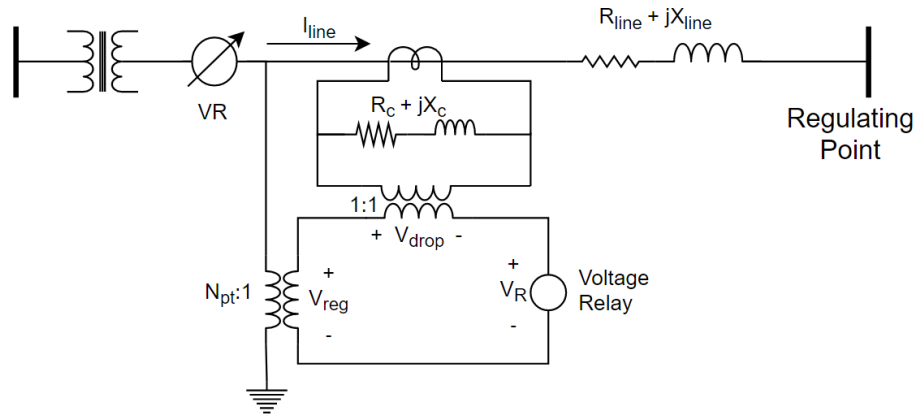


Figure 2.3 A typical voltage regulator control mechanism.

2.3.2 Indirect voltage control in PDS

Reactive power is needed for most of the load types in DSs, and decent reactive power flow management is an important issue in order to have reliable and secure distribution systems. Traditionally reactive power compensation is achieved by connecting shunt capacitors at nodes where there is big reactive power demand. ShCs can be installed either at the substation site or along the feeder with a fixed or variable Var compensation capacity. This

on-site supply method results in reduction of the feeder power losses and of the voltage drop. Fixed type ShCs have constant reactive power injection capacity, and they operate an on and off strategy based on high or light load seasons, respectively. On the other hand, switched type capacitors have variable injection capacity which can be adjusted according to required reactive power. In terms of superiority, switched type capacitors are better since they can provide more precise and flexible compensation compared to fixed types capacitors.

The amount of reactive power injection to the system can be calculated as:

$$Q_C = Q_{C,rat}V^2 \quad (2.4)$$

where

- Q_C is the reactive power injected by the capacitor in MVar;
- $Q_{C,rat}$ is the MVar rating of the capacitor; and
- V is the voltage in pu (relative to the capacitor voltage rating).

As mentioned above, the reactive power injection will improve the voltage profile and decrease the voltage drop of the feeder as shown below in an approximated equation:

$$\Delta V \approx \frac{(R_{Line}P_L + X_{Line}(Q_L - Q_C))}{V} \quad (2.5)$$

In addition to the reduction in voltage drop, proper reactive power compensation results in power loss reduction by decreasing the current as:

$$I = \frac{\sqrt{P_L^2 + (Q_L - Q_C)^2}}{V} \quad (2.6)$$

$$P_{Loss} = I^2 R_{Line} \quad (2.7)$$

2.3.3 Overview of different VVC methods used in PDS

Voltage violation is among the most severe power quality problems in distribution systems; therefore, many researchers have been devoted to tackling this problem, either at the planning or operational level. Different aspects of the VVC problem have been investigated by proposed algorithms in the literature, such as control device placing, sizing, operational scheduling, and coordination along with many other aspects.

In the planning stage, the determination of capacitor size and placement are two main key factors in having optimum Var control. Capacitor banks are expensive devices and cannot be placed randomly along the feeder, therefore different capacitor placement and sizing algorithms are proposed to maximize the benefits [12–14]. In [14], a new formulation of the general capacitor placement problem is presented to maximize the benefits of reactive power compensation. During problem formulation, the authors considered practical aspects of capacitors, loads and operational constraints. The problem is simulated under different load levels to determine the locations, types, sizes and control settings of the capacitors. Another placement approach is presented in [15], where candidate buses are selected based on loss sensitivity factor, and the size of capacitors is found using the particle swarm optimization (PSO) technique. The loss sensitivity factor basically defines the candidate bus, where the biggest loss reduction occurs when a capacitor is placed on it.

There are also papers that investigate the VVC problem at the operational level. For instance, in [11], the authors present a VVC method that uses fixed/switched capacitors and VRs to minimize peak power demand and energy loss. Reactive power compensation is not always sufficient, so the VRs are also utilized for voltage regulation. Much like the

capacitors, the VRs' locations and minimum required number are also determined.

There are also VVC algorithms where load curve is divided into load levels, and the VVC problem is optimized in each load level [16–18]. In [16], a day-ahead load forecast is partitioned for an offline coordinated VVC. In [17], the load curve is partitioned into 24 discrete states (one for each hour) without load clustering, unlike the case in [16], and for each load state, the operation of control devices is optimized using GA.

To have a proper voltage profile, a coordination between control devices is crucial, and it is also critical for avoiding unnecessary switching operations. These stated issues have been covered in literature by several authors [11–13, 19]. There are three coordination methods; manual, automated, and reactive power device control modes. In early stages of coordination, manual control mode was used, where operators are directly in charge of dispatching the capacitors and OLTCs [20]. Manual operation mode is not economical due to the personnel requirement on site. Manual control mode is used only if there is a need for operator interruption under some circumstances. On the other hand, in automated mode, the tap positions of the OLTC are changed by the AVR, which responds to the change in secondary bus voltage. A third method is to use the reactive power device control mode, which detects the reactive power flow over the main transformer and determines if it is necessary to switch the capacitors on/off. For instance, the coordinated VVC control at a substation is studied in [21], wherein OLTC and VR are controlled in the centralized mode, and the bandwidth (BW) of VR changes adaptively as the system load changes.

2.4 Impacts of RESs on Distribution Systems

In recent decades, renewable energy resources penetration level has been increased due to many different economic and environmental benefits. This high-level penetration of

RESs brings important challenges and opportunities to the existing DS operation practices. Traditional VVC control methods are no longer reliable for the new types of DSs under high RESs integration. Thus, RESs' impact on the system has to be taken into account in order to have optimum VVC algorithms in ADSs. Furthermore, renewable DGs have begun to be used in control algorithms, and they also need to be coordinated with the available control equipment in order to ensure proper voltage regulation. The impact of renewable DG's on voltage profiles and the VVC problem are explained in the next two subsections.

2.4.1 RES impacts on voltage profile

RESs can be connected to the system either by using synchronous/induction generators or by using a power electronic interfaces. A one line illustration of the feeder with RESs is shown in Fig 2.4. RESs are mainly used for active power generation, but in some operation modes, they can also inject/absorb reactive power. If RES power interchange is included in the approximated voltage drop equation, the equation (2.3) will be as follows:

$$\Delta V = V_1 - V_2 \approx \frac{(R_{Line}(P_L - P_{DG}) + X_{Line}(Q_L - (\mp Q_{DG}))}{V_2} \quad (2.8)$$

Equation (2.8) indicates that, if an RES generates active power in excess of the feeder load, power flow will be from the RES-connected node to the substation and the connected bus voltage will increase. On the other side, RES reactive power absorption decreases the connected bus voltage, while reactive power injection increases the voltage at the connection bus.

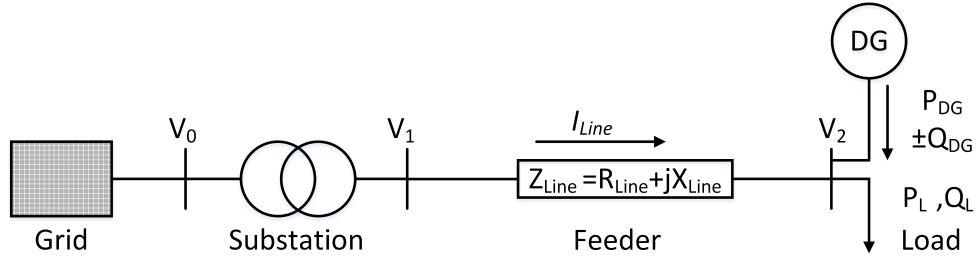


Figure 2.4 Simple one-line diagram of a feeder with a RES connected to the feeder-end.

2.5 Volt/Var Control in Active Distribution Systems

As stated theoretically in equation (2.8), active and reactive power injection from RES means a voltage rise problem if not tackled properly at the connection point.

In the literature, many different techniques and approaches have been proposed to solve the VVC problem for ADSs [3–7]. Each technique either uses only a single control device, or a combination of available existing control devices (e.g. OLTCs, switched/fixed ShCs, and VRs), and emerging control variables, such as electrical energy storage systems (EESSs), or the real and reactive power of DGs.

The IEEE Standard 1547 does not allow DGs to participate in voltage control actively due to their intermittent output power. Therefore, DSOs force DGs to operate at unity power factor or in voltage control mode, and do not allow them to participate in VVC [9]. However, in recent decades the approach of DSOs has evolved, and in some countries, DGs are already required to provide active voltage regulation by acting as a control devices [22–27]. VVC algorithms in ADSs can be categorized in two groups; local and centralized VVC algorithms.

2.5.1 Local VVC methods in ADSs

Local Volt/Var control methods use only local measurements and do not need any information about the whole system status to determine their control actions as it is illustrated in Fig 2.5. Control devices adjust their set points based on their terminal voltages, so no communication is needed between the nodes, thus control algorithm operation cost is low.

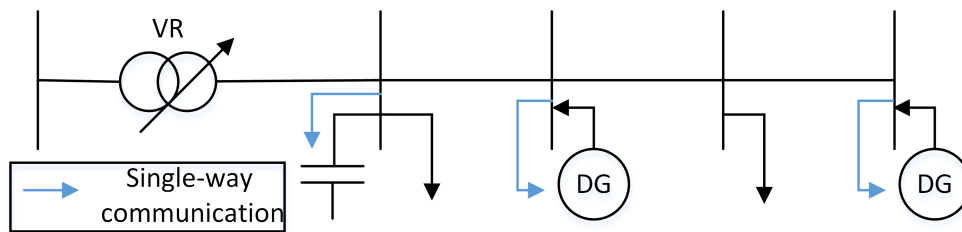


Figure 2.5 Simple one line representation of local VVC.

Wind-based DG is used for voltage regulation in [28], by assuming that it can operate in two modes; power factor mode or voltage control mode. The operation mode is decided based on the measured terminal voltage at the generator connection point. During normal operation (the measured terminal voltage is within the limits), the power factor mode is activated to obtain greater system operation savings. On the other hand, if the measured terminal voltage is out of limits, then the voltage control mode is adopted. Active power curtailment, which is not economical for DG owners, is considered as a last option for cases in which the previous two operation modes are not sufficient.

Sensitivity analysis determines how DG's power injection or absorption will affect feeder voltage, and it has also been employed to define setting points for DGs. An example of sensitivity analysis for a local voltage control strategy is presented in [29]. The same approach is optimized by using a multi-objective genetic algorithm to minimize the active power losses and reactive power exchanged between DS and the DG units in [30].

The authors of [31] presented a VVC approach that combines local and remote VVC methods to minimize the system losses. To compare their proposed method with conventional ones, they used both constant (small hydro power) and variable (wind power) dispatch-able power of DG. The proposed algorithm can be separated into three main steps. First, the OLTC set positions and capacitor status are scheduled based on a one-day load forecast. Second, dynamic programming based optimization is used to determine the optimum tap position and the status of OLTC and capacitors. Finally, they compared steps 1 and 2, and defined a set of remote schedules. The implementation of local-remote control increased the number of OLTC operations, so they put constraints on the OLTCs with a maximum daily number of operations.

Another local decentralized reactive power management strategy to maximize the active power generation of the distributed renewable energy resources is presented in [32]. If a voltage violation occurs at the point of interconnection of DG, the first action is to try to bring the voltage back into the allowed range by using reactive power compensation. If the first option is not sufficient to correct the voltage, then active power curtailment is considered as a last resource. The objective function is to minimize the reactive power injection by the DGs, while system losses are not considered as an objective which is very important in DSs.

2.5.2 Coordinated VVC in ADSs

A second type of VVC algorithm is the coordinated (centralized) VVC type as a basic schematic as shown in Fig 2.6. Coordinated VVC depends on reliable communication links, smart measurement devices, and strong programmable control units. The basic control flow happens as follows:

- Sensor devices measure the status of their terminal and send the measurements to the central computer via communication links;
- The centralized algorithm solves the optimization problem by using received measurements; and
- Calculated control action commands are sent back to the slave control devices.

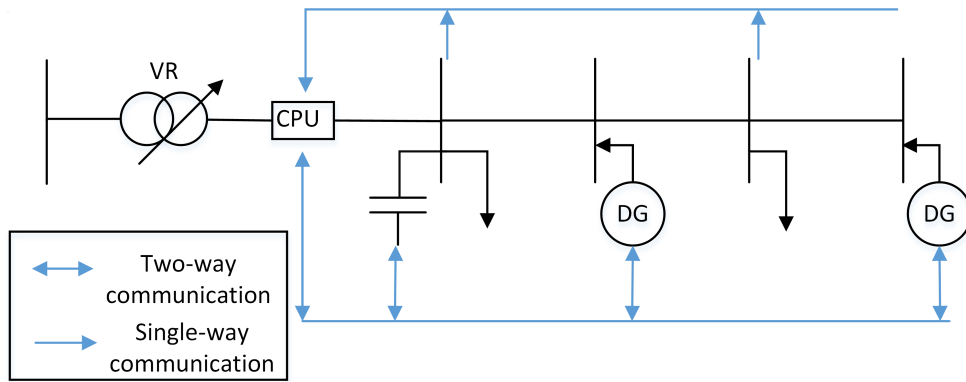


Figure 2.6 Simple centralized VVC Schematic.

Coordinated VVC methods are the focus of widespread and ongoing attention from researchers, and as such many coordinated algorithms have been proposed in the literature. A coordinated VVC algorithm is formulated and implemented in [7], which minimizes the real power drawn from the substation, and ShCs. VR and reactive power of DG are used as voltage controllers. DG units are represented as a unit with specified real and controllable reactive power outputs. The proposed algorithm reduced the real power demand by 6% more than traditional control algorithms.

In [33], OLTC transformers and switched ShCs are coordinated to improve the voltage profile for a system, in which renewable DGs are considered as voltage-independent active power injection with zero reactive power injection. The authors also show that the higher

the DG penetration is, the greater the OLTC tap operation, meaning more wear and tear on the OLTC taps. The proper PV generator bus selection is also defined, and by placing PV generators at different buses they investigate the impact of PV location on the number of switching operations for the OLTC transformers. Finally, they state that in terms of economic concerns, the appropriate bus to place a PV on is where the least switching occurs.

In [23], the authors proposed a coordinated online voltage control algorithm that uses sensitivity matrices between P-V and Q-V. Since in DSs it is not possible to regulate all buses directly with control devices, some critical buses are selected for voltage regulation based on sensitivity matrices. The reactive power of DG is used as a first option, and if the voltage is still exceeds limits after the first actions, then OLTC is used to regulate the voltage.

Tackling the large DSs and control entities makes the search space very massive for optimization and the computation takes a long time, which is a limitation for online voltage control. Therefore, as a solution to this problem, [34] presents a three-stage adaptive online coordinated voltage control with a very fast response time. The response time is decreased by utilizing accumulated knowledge to reduce search space. The knowledge is obtained from offline long-term optimization and online experiences.

Some papers, such as [35] and [36], use the categorization of available control devices based on different criteria (e.g., cost, response time) to coordinate them optimally. In [35], the control actions are categorized as either master or slave. Control devices which are designated as "master" are the first to act against voltage violations, and the "slave" control devices will follow the masters if necessary.

In [37], DGs actively participate in steady-state voltage control with OLTCs and ShCs.

The objectives of these methods are to decrease the number of switching operations and reduce the power losses. The DG output is dispatched for the next day according to the day-ahead load forecast. Firstly, the authors developed an algorithm suitable for dispatchable DG, which is capable of producing controllable active power on demand. The algorithm is also evaluated based on non-dispatchable DG types like wind and solar generators.

[38] presents a coordinated VVC algorithm that is computationally efficient at the expense of optimality for large radial distribution networks. The algorithm consists of two separate but dependent objectives; one, to have an optimum power factor and determine optimal scheduling for the ShCs, and two, to flatten the voltage profile, adjust the VR and transformer tap ratios for a 24-hour scheduling cycle.

Some papers are particularly interested in distribution systems with renewable PV generation and its impacts on operations of other control devices. For instance, [39] investigates the detailed impacts of PV on VR and OLTC, and proposes a coordinated control strategy to eliminate the negative effect of PV by using reactive output power from PV. The OLTC and PV control settings are calculated based on the day-ahead radiance and load profile forecast. The VR is considered in an autonomous mode, but the OLTC and PV generation plants are coordinated to minimize the number of tap switching operations.

Recent developments in battery systems make electric energy storage systems (EESSs) more feasible to use in distribution systems. Particularly, EESSs have started to be utilized in VVC algorithms, and their coordination with OLTC is commonly studied in literature [3,40–42]. In [3], a coordinated voltage control scheme is presented, which integrates EESS with OLTCs for planning. The algorithm relies on a voltage sensitivity factor and voltage cost sensitivity matrix. In [40], the main objective is to use EESS to relieve the stress on OLTC and decrease the resistive power losses under high PV penetration. In [41], PV and battery energy storage (BES) are coordinated in order to address voltage rise problems.

In [42], probabilistic estimation of PV generation and randomness in load are modelled to characterize the effective utilization of BES. Uncertainties in PV generation and load forecast are also considered in the characterization.

Normally, the optimum reference schedule for control settings is created according to day-ahead forecast data, which may contain a big forecasting error. Therefore, the error associated with the forecast plays an important role in terms of obtaining an optimum solution. Particularly, in renewable DGs, the error becomes more crucial than traditional generation units. Therefore, an optimal voltage control algorithm that takes into account forecast errors of PV generation is presented in [43]. They introduced a new technique; re-forecasting the PV generation and re-calculating optimum control reference settings based on re-forecasted data with less forecast error.

Dividing distribution feeders into control zones is also a commonly used method utilized in VVC algorithms. The basic purpose of zoning is to provide a more-efficient operation. A coordinated voltage control method according to the concept of zoning is presented in [44]. The determination of control zones relies on sensitivity analysis rather than on the electrical distance used in other zone-based papers. The control devices are prioritized based on their operational cost, and if a device is cheaper, then its control zone will be larger.

Coordination between control devices for unbalanced distribution systems was first explored in [45]. The optimization problem has been divided into two stages; stage 1 is a one-day ahead optimization procedure, that depends on load and generation forecast and provides a reduced search space for stage 2, and stage 2 is a local optimization procedure that requires present load and generation levels obtained through forecasting or direct measurement.

In [46], an online voltage control approach that relies on real-time measurements by remote terminal units (RTUs) is proposed to investigate the impacts of load curtailments on voltage profiles. According to the measurements, the tap positions and required load curtailments are determined for different system conditions. In normal conditions, the voltage control is performed according to a pre-scheduled voltage control program, which is carried out during the day-ahead operational scheduling. In emergency conditions, a demand response program provides incentive payments to customers for reducing their loads. The assumption in the study is that responsive loads have already signed their participation contract, and participants are selected by the DSO online. The authors used minimum and maximum voltage estimations for control, as in [8]. RTUs are installed at DGs or capacitor buses for collecting field data and sending it back to the master station. The proposed algorithm is tested under two cases; one, unpredictable wind and load fluctuations and two, wind turbine outages. The first scenario uses a tap changer for voltage control, and the second, which is an emergency state, where the tap changer program could not bring the voltages into range, uses demand response, which is basically power curtailment.

2.6 Conclusion

This chapter provides background information about factors that have an impact on system voltage profiles. The chapter also presents an overview of various Volt/Var control algorithms in both passive and active distribution systems. The benefits and challenges of local and coordinated volt/Var control algorithms are also discussed. It is well understood in the literature that coordinated voltage control techniques provide better results than the decentralized (distributed) control algorithms. However, coordinated algorithms require a

well-established communication structure throughout the distribution networks.

Chapter 3

State-based Volt/Var Control Algorithm for Active Distribution Networks

3.1 Introduction

In this chapter, we first identify the system state index based on the voltage profile, and present the transaction scheme between states. Next, we formulate the bus stability index to identify the weakest bus in the system, and voltage sensitivity analysis of the buses. Furthermore, we formulate the cost of control devices, objective functions, and constraints, and the proposed rule-based algorithm for the emergency state is presented.

In the simulations section, the optimization algorithm used in solving the proposed VVC problem with the Pareto optimality are discussed and presented. Next, the forecasting model for wind power generation is discussed with consideration of forecast error. Then,

the proposed state-based VVC algorithms are tested on IEEE-34 and IEEE-123 bus radial distribution test systems to verify the effectiveness of the developed algorithm. Finally, different scenarios are simulated and the results are analyzed and presented.

3.2 System State Index (SSI)

Distribution systems may not sustain normal-state operation over time and could slip into abnormal operating conditions, in which voltage abnormalities play an important role. System voltage monitoring and preventive/corrective actions are thus crucial for sustaining normal-state operation. American National Standard Institution (ANSI) C84.1 specifies boundaries and ranges (Range A and B) for utilization voltage (Fig. 3.1). Range A is recommended for normal operating voltages, while range B identifies acceptable, but less optimal voltage values. For this study, voltage range C represents a system in an emergency (abnormal) state, which may result in curtailment of DG output power or service interruptions. It is worth mentioning that, the term of emergency state is used here as a state, in which the control actions should be taken as soon as possible, and it is not related to power system stability.

In this study, it is assumed that real-time voltage measurements of critical buses are measured and sent to a central computer, and those received voltages are used to obtain the system state index (SSI), given in (3.1). The criteria for determining critical buses

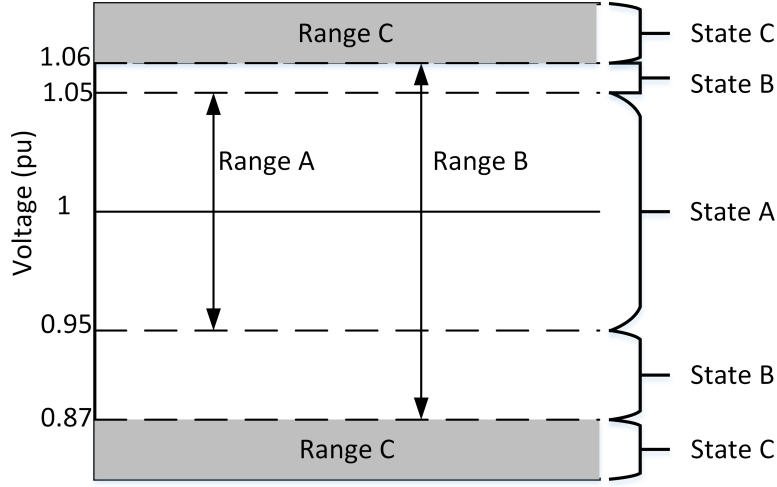


Figure 3.1 Illustration of voltage boundaries and ranges specified by ANSI C84.1

where the minimum and maximum voltages occur is adopted from [8].

$$SSI = \begin{cases} A, & \text{if } 0.95 \leq V_{i,t} \leq 1.05, \forall i, t \\ B, & \text{if } 0.87 \leq V_{i,t} < 0.95 \text{ or } 1.05 < V_{i,t} \leq 1.06, \\ C, & \text{if } V_{i,t} < 0.87 \text{ or } 1.06 < V_{i,t}. \end{cases} \quad (3.1)$$

3.2.1 System operating states

Based on the SSI, the system is identified as one of three operating states; normal (State A), intermediate (State B), and emergency states (State C), as shown in Fig. 3.2. The states can be explained as follows:

- **State A** is the normal state in which all critical bus voltages are within range A. In this state, the primary goal is to operate the system in the most economical way by formulating the VVC problem as a multi-objective nonlinear optimization. The

objectives are specified to minimize active power losses and control action costs while maintaining the minimum number of switching actions.

- **State B** is the intermediate state in which at least one bus voltage falls into region between range A and C. The primary goal is to bring the system back into the normal state and prevent it from falling into the emergency state. The problem is formulated as a multi-objective optimization with different objectives of minimizing voltage violation and active power losses.
- **State C** is the emergency state in which at least one bus voltage is in the range C. The primary goal is to bring the voltage back within the range B limits in a reasonable time. The emergency state is associated with the greatest possibility for the system to deteriorate into load shedding or service interruption, so identifying the weakest bus is vital for protecting the system. The node with the lowest bus sensitivity index (BSI) is the most sensitive one to load shedding or service interruption. The BSI presented in [47] has been adopted to identify the system's weakest bus and it is presented in detail in Section 3.3.

3.2.2 State switching

In response to either a disturbance or control action, a distribution system can switch from one state to another (Fig. 3.2). Transitions between states are indicated by either inner or outer loop arrows representing disturbances and control actions, respectively. Any arrow in the inner loop (1, 2 and 3) can signify any type of disturbance that weakens system stability, whereas any arrow in the outer loop (4, 5 and 6) denotes a controlled transition resulting from a control action taken.

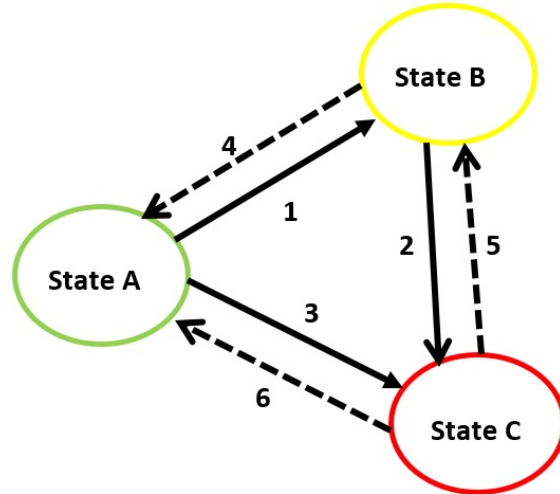


Figure 3.2 System state-switching scheme

The following points explain the outer loop arrows:

1. **Arrow 4** represents a transition from state B to state A, using specified control devices. The objectives are to minimize both the voltage violation and the control action cost. The primary goal is to accomplish the transition in the most economical manner.
2. **Arrow 5** represents a transition from state C to state B, through the application of a rule-based control strategy, which requires fast and effective control devices. Since the objective is to bring the system into state B as soon as possible, the cost function of the control devices is neglected and used according to priority list. The only objective is to minimize the voltage violation.
3. **Arrow 6** represents a transition from state C to state A through the application of a rule-based control strategy, whereby fast and effective control devices are used

according to priority list. The objective is to bring the system into state A as quickly as possible by eliminating all voltage violations and securing the system.

After each control action, the system status is redefined, and if the state transaction has occurred, then a new state-related control strategy is adopted by the algorithm for the next optimization hour. The proposed state-based VVC algorithm flowchart is shown in Fig. 3.3.

3.3 Bus Sensitivity Index (BSI)

It is important to define the system's weakest bus to service interruption to be able to act quickly and effectively when the system is in emergency state, since it may trigger abnormalities in the system that may lead to service interruptions. Thus, the bus sensitivity index (BSI), which is presented in [47], is adopted to identify the weakest bus in the system, so the proper preventive actions can be taken to protect the system from service interruption. The BSI is based on transferred active and reactive power equation of a distribution line.

3.3.1 Mathematical model of the BSI

Let us consider the two-bus (sending and receiving bus) network shown in Fig 3.4 and write the real and reactive power at the receiving bus end as follows:

$$P = \frac{V_s V_r}{|Z|} \cos(\theta_z - \delta_s + \delta_r) - \frac{V_r^2}{|Z|} \cos(\theta_z) \quad (3.2)$$

$$Q = \frac{V_s V_r}{|Z|} \sin(\theta_z - \delta_s + \delta_r) - \frac{V_r^2}{|Z|} \sin(\theta_z) \quad (3.3)$$

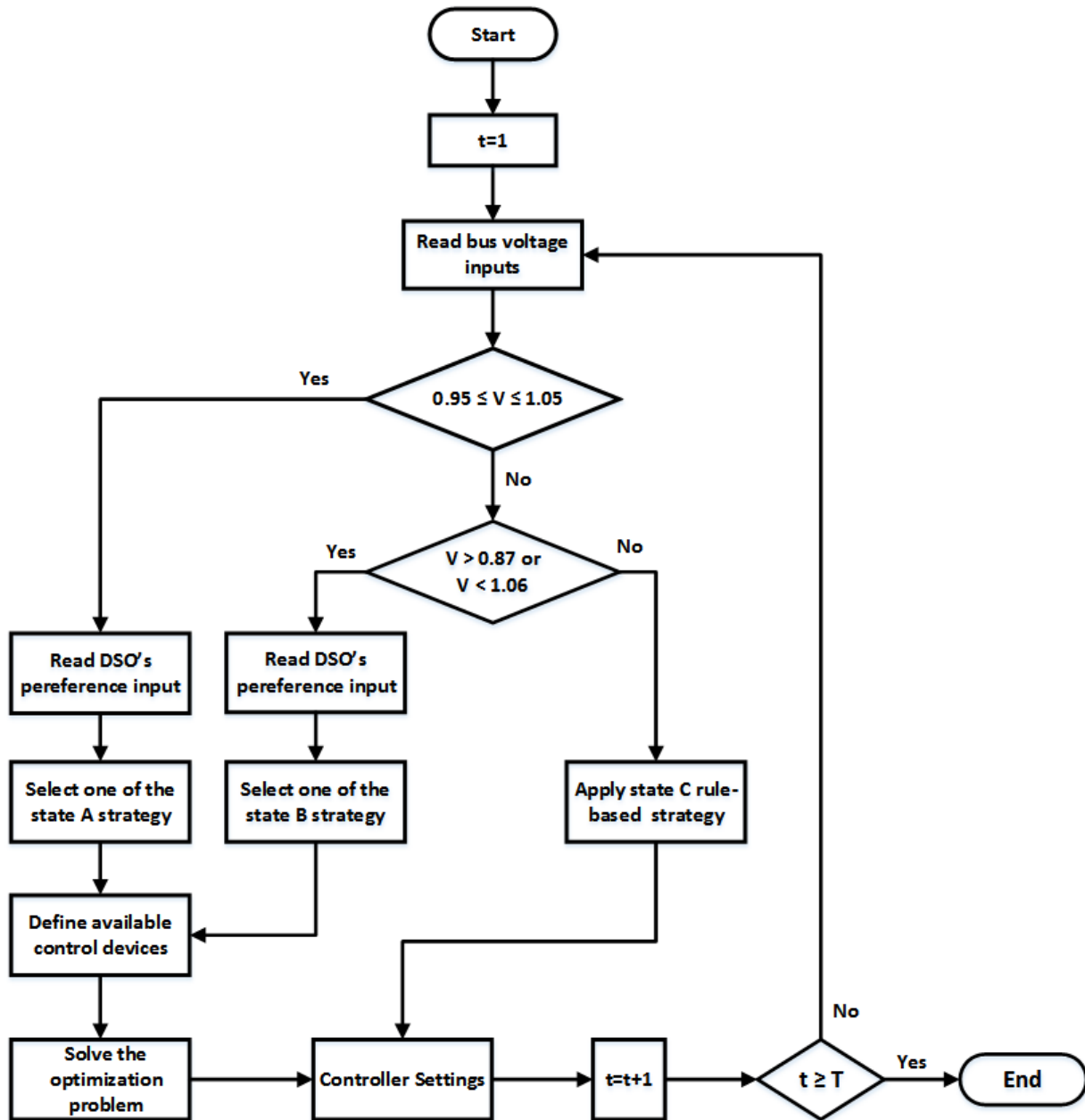


Figure 3.3 Flowchart of the proposed state-based VVC algorithm

where V_s and V_r stand for phase voltage magnitudes of sending and receiving bus, respec-

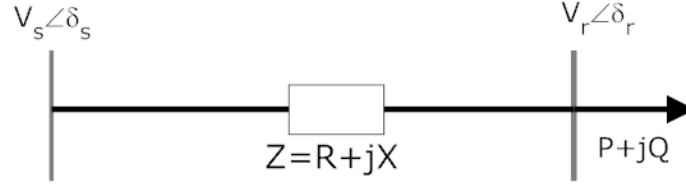


Figure 3.4 One line diagram of a two-bus distribution network.

tively, and Z is the line impedance, and θ_z , δ_s and δ_r represents phase angle of the line impedance, sending bus voltage, and receiving bus voltages, respectively.

Trigonometric identity ($\cos^2(a) + \sin^2(b) = 1$) and squared summation of equations (3.2) and (3.3) yield a well-known bi-quadratic equation as:

$$V_r^4 + V_r^2[2(PR + QX) - V_s^2] + (P^2 + Q^2)|Z|^2 = 0 \quad (3.4)$$

From equation (3.4), active and reactive power at the receiving end of the line can be rewritten as:

$$P = \frac{-\cos(\theta_z)V_r^2 \pm \sqrt{\cos^2(\theta_z)V_r^4 - V_r^4 - |Z|^2Q^2 - 2V_r^2QX + V_s^2V_r^2}}{|Z|} \quad (3.5)$$

$$Q = \frac{-\sin(\theta_z)V_r^2 \pm \sqrt{\sin^2(\theta_z)V_r^4 - V_r^4 - |Z|^2P^2 - 2V_r^2PR + V_s^2V_r^2}}{|Z|} \quad (3.6)$$

The following conditions need to be satisfied to have real and reactive power at the receiving end:

$$\cos^2(\theta_z)V_r^4 - V_r^4 - |Z|^2Q^2 - 2V_r^2QX + V_s^2V_r^2 \geq 0 \quad (3.7)$$

$$\sin^2(\theta_z)V_r^4 - V_r^4 - |Z|^2P^2 - 2V_r^2PR + V_s^2V_r^2 \geq 0 \quad (3.8)$$

Summation of equations (3.7) and (3.8) gives:

$$2V_s^2V_r^2 - V_r^4 - 2V_r^2(PR + QX) - |Z|^2(P^2 + Q^2) \geq 0 \quad (3.9)$$

which is the bus sensitivity index (BSI) for receiving end bus and represented as:

$$BSI(r) = 2V_s^2V_r^2 - V_r^4 - 2V_r^2(PR + QX) - |Z|^2(P^2 + Q^2) \geq 0 \quad (3.10)$$

The BSI defines the weakest bus, which is the most sensitive bus to the service interruption in the system in the emergency state (State C).

3.4 Voltage Sensitivity Analysis

Optimization algorithms cannot be used in emergency states because of excessive computational burden; therefore, the sensitivity of bus voltages to control actions plays a key role in determining optimal control device settings. The voltage sensitivity of each node within the control zone of particular control devices, namely the OLTC, the voltage regulator, and the reactive and active power of DG, is calculated as proposed in [48]. Based on the control zone of a particular device, sensitivity values are calculated as follows: i.) for 1-phase voltage regulators, only the sensitivity of downstream nodes which are connected to the

same feeder is calculated, ii.) for DGs and capacitor banks, the sensitivity is calculated for all feeder nodes. The voltage sensitivity of the i^{th} bus to a tap change in the j^{th} OLTC or voltage regulator is expressed as κ_{ij} , while the sensitivity of the same bus to changes in the reactive and active DG power is expressed as μ_{ig} and ρ_{ig} using numerical differentiation as it is shown in (3.11):

$$\begin{aligned} \kappa_{ij} &= \frac{\Delta V_{ij}}{\Delta Tap_j}, \quad \mu_{ig} = \frac{\Delta V_{ig}}{\Delta Q_{DG_g}}, \quad \rho_{ig} = \frac{\Delta V_{ig}}{\Delta P_{DG_g}} \\ i &= 1, 2, \dots, n; \quad j = 1, 2, \dots, m; \quad g = 1, 2, \dots, N_{DG} \end{aligned} \quad (3.11)$$

where ΔV_{ij} is the voltage change in bus i for the tap change in VR j , and ΔV_{ig} is the the voltage change in bus i for the DG's active/reactive power change. To calculate each bus voltage's sensitivity to a given controller, that controller's settings are changed incrementally while all other controllers' settings are fixed. Based on the recorded voltage change the sensitivities are calculated for each control devices (OLTC, VR, and DG), such as the sensitivity of bus voltages for tap, kW or kVAr change. Voltage sensitivities are dependent on the topology and impedance of the network [48]. Therefore, as long as the topology and the network impedance maintained constant, there will be no need to recalculate voltage sensitivities. In this study, the sensitivity indices are calculated for each hour of a day (different loading conditions), and we have observed that the sensitives of the bus voltages to each control device do not change as the load changes. The sensitivities are calculated and stored ahead of time, considering the network topology stays fixed for the next 24 hours. If the network topology and impedance change, the sensitivities need to be recalculated to replace the stored values. For real-time implementation of the algorithm, such updates should be made on an ongoing basis by continuous tracking of system information. A control device priority list for each bus, to use in emergency states, is also obtained by

ordering the sensitivity values for that bus in descending manner.

3.5 Control Devices

A number of control devices can be used in VVC problems, such as, OLTC transformers, voltage regulators, fixed or switchable capacitor banks, static VAR compensators, electric energy storage systems, DG's controllable active and reactive powers. Control devices can be categorized as two main classes; voltage control devices and reactive power control devices. Voltage control devices have a primary impact on voltage and a limited effect on reactive power flow such as OLTC, voltage regulator, and active power of DG.

On the other hand, static VAR compensator (SVC), fixed or switchable capacitor banks, and reactive power of DG are classified as reactive power control devices, and these devices have their main effects on reactive power flow of the system.

3.5.1 Cost Functions of Control Devices

In terms of economic aspects, voltage control actions are associated with an undesirable cost of setting adjustments (action cost) of control devices. Without considering the action cost, the claimed optimality in control algorithms may not be a real optimal solutions in terms of economical concerns. For an economically optimal solution, the action cost for each control devices should be considered as well.

3.5.1.1 On-Load Tap-Changer (OLTC)

Power transformers equipped with OLTCs are the main components of distribution network voltage control. Therefore, operational reliability of OLTCs is extremely important for

reliable system operation. Over time, OLTCs' mechanical components wear out and require maintenance. The principle of defining maintenance time is based on either the time elapsed in service or the number of tap operations, whichever comes first. In conventional types of OLTCs, the maintenance interval typically is 7 years or between 50,000 and 100,000 tap operations [49].

Multiple methods are used to define the cost of OLTC operation. In this work, the cost function presented in [3] has been adopted for the OLTC action cost which basically depends on the estimated lifespan and total number of tap operations during the whole service life. Therefore, a generic action cost is given by:

$$C_{OLTC} = \frac{C_{OLTC}^R}{N_{OLTC}^R} (\$/tap) \quad (3.12)$$

where the number of tap operation remaining time is:

$$N_{OLTC}^R = \frac{LS_{OLTC}^R}{LS_{OLTC}^T} N_{OLTC}^T \quad (3.13)$$

It is worth mentioning that for OLTC cost calculation the maintenance cost has not been considered. In the simulations section, the cost of a single tap operation was adopted from [50] to be 1.40 \$/tap.

3.5.1.2 Shunt capacitor banks (ShCs)

The purchase cost per kVAR rating of shunt capacitors is fixed and defined as [51]:

$$C_{ShC}^t = C_{ShC}^f / LT_{ShC} \quad (3.14)$$

3.5.1.3 Cost of DG active power curtailment

In the power market, a renewable DG owner's first goal is to maximize their profit by selling as much produced power as possible to the utilities. DGs with inverter equipment can control the active power injected into a system under some critical conditions (e.g., if voltage rises, the active power can be ramped down and DGs can sometimes even be disconnected from the grid). The active power curtailment of DGs causes monetary losses for DG owners, which is defined as the control cost of DG's active power:

$$C_{DG}^P = C_e P_{curt.} \text{ (\$)} \quad (3.15)$$

The curtailed DG active power cost will be the multiplication of curtailed power and the contract price set out; for example, the price is 12.8 ¢/kWh in Ontario [52]. The total operational cost T_{Cost} of the system for T intervals is calculated as follows:

$$T_{Cost} = \sum_{t=1}^T \left(C_{DG,t}^P + C_e P_{loss}^t + C_{ShC}^t Q_{ShC,t} + C_{OLTC} \Delta tap_t \right) \quad (3.16)$$

3.6 Problem formulation

VVC optimization can involve a number of objectives, and trying to optimize all objectives simultaneously may result in unacceptably long computational times and suboptimal solutions; therefore, objectives are prioritized according to the system state. For each state, its specified objectives are used either in the single/multi-objective optimization or in the rule based algorithm. Although the literature reports examinations of many different objectives, this study considers only those most commonly used. However, DSOs can define other objectives as needed and include them for consideration. The objectives are classified

as either system or device ones.

3.6.1 System Objective Functions

System objective functions are targeted at the minimization of two factors; power loss and voltage deviation.

3.6.1.1 Power loss minimization

The objective function of loss minimization is formulated as in (3.17) which tries to minimize the power losses in the distribution system for a specific time period:

$$\min P_{loss} = 0.5 \sum_{t=1}^T \sum_{i=1}^n \sum_{j=1}^n (G_{ij} [V_{i,t}^2 + V_{j,t}^2 - 2V_{i,t}V_{j,t} \cos(\delta_{j,t} - \delta_{i,t})]) \quad (3.17)$$

3.6.1.2 Voltage deviation minimization

The objective function for minimizing voltage deviation is formulated as follows:

$$\min V_D = \sum_{t=1}^T \sum_{i=1}^n (V_{i,t}^{set} - V_{i,t}^m)^2 \quad (3.18)$$

3.6.2 Device Objective Functions

In distribution systems, high penetration of renewable DGs causes excessive tap switching due to DGs' high output variability [33]. This excessive movement increases operational costs due to increased maintenance requirements, and results in reducing OLTCs' total

service life, which is not cost-effective. For a monetarily global optimal solution, the control actions' cost functions are considered.

3.6.2.1 Number of tap movement minimization

The minimization of tap movement can be expressed as follows:

$$\min \sum_{t=1}^T \left(C_{OLTC} \Delta tap_t \right) \quad (3.19)$$

where $\Delta tap_t = \sum_{i=1}^m |tap_{i,t+1} - tap_{i,t}|$, m is the total number of VR in the system.

Capacitor cost is important if the shunt capacitors are switched-type; however, our simulations neglected cost because the capacitors are fixed-type or already in the system.

3.6.2.2 DG active power curtailment minimization

The minimization of active power curtailment is also an important objective with respect to monetary losses. It is expressed as the difference between available and injected active power into the grid, as follows:

$$\min \sum_{t=1}^T (P_{DG,t}^f - P_{DG,t}^{inj}) \quad (3.20)$$

3.7 Constraints

The methodology involves the following constraints.

3.7.1 Node power flow constraints

Equality of generation and load power is given by:

$$P_{gi,t} - P_{li,t} = V_{i,t} \sum_{j=1}^n V_{j,t} (G_{ij} \cos(\theta_{ij,t}) + B_{ij} \sin(\theta_{ij,t})), \quad \forall i, t \quad (3.21)$$

$$Q_{gi,t} - Q_{li,t} = V_{i,t} \sum_{j=1}^n V_{j,t} (G_{ij} \sin(\theta_{ij,t}) + B_{ij} \cos(\theta_{ij,t})), \quad \forall i, t. \quad (3.22)$$

3.7.2 Bus voltage limits

Bus voltages are constrained as:

$$V_i^{min} \leq V_{i,t} \leq V_i^{max}, \quad \forall i, t. \quad (3.23)$$

3.7.3 Capacitor reactive power output limits

For switchable capacitors the reactive output power is constrained as:

$$Q_{ShC_i}^{min} \leq Q_{ShC_i,t} \leq Q_{ShC_i}^{max}, \quad i = 1, 2, 3, \dots, Cn \quad (3.24)$$

3.7.4 Transformer tap position constraints

Transformer tap position is constrained as:

$$Tap_i^{min} \leq Tap_{i,t} \leq Tap_i^{max}, \quad i = 1, 2, 3, \dots, Tn \quad (3.25)$$

3.7.5 DG constraints

Distributed generator units equipped with electronic interfaces can modulate their reactive and active power (injection or absorption). Normally, the reactive and active limits of DG units will be governed by converter current and voltage limits, and will also depend upon the generator size and type [32]. Bus voltage (V), power factor (PF), active and reactive power (P and Q, respectively) values are constrained by lower and upper limits for each time interval, as follows:

$$V_i^{min} \leq V_{i,t} \leq V_i^{max}, \quad i = 1, 2, 3, \dots, DG_n \quad (3.26)$$

$$Q_{DG_i}^{min} \leq Q_{DG_{i,t}} \leq Q_{DG_i}^{max}, \quad i = 1, 2, 3, \dots, DG_n \quad (3.27)$$

$$P_{DG_i}^{min} \leq P_{DG_{i,t}} \leq P_{DG_i}^{max}, \quad i = 1, 2, 3, \dots, DG_n \quad (3.28)$$

3.8 Rule-Based Emergency State VVC Algorithm

A rule-based (RB) algorithm (Fig. 3.5) is proposed for emergency states so that quick actions can be taken, prior to power discontinuity, to bring all bus voltages back into State B or A, as follows:

1. Determine the system's weakest bus using the bus sensitivity index (BSI) (bus i).
2. Look up the bus i control device priority list and choose the most effective controller, which is the one with the highest sensitivity to the bus i (control device j).
3. Calculate the required action for control device j to alleviate the voltage violation at bus i by sensitivity Eq. (3.11).

4. Ensure that the required action creates no new violations. If it does, then modify (decrease/increase) the required action until it creates no voltage violation.
5. Check if the voltage V_i at bus i is still in range C . If so, then check if control device j reached the limits; if it did, then switch to the most effective control device (control device j), which comes after the used one in the priority list, and repeat steps 3-5 until the bus i voltage violation is eliminated.
6. After bus i voltage violation has been eliminated, check if the system is in state C .
7. If so, go to step 1. Otherwise, go to step 8.
8. Stop and switch to new state-related control algorithm.

The flowchart for the proposed rule-based algorithm is shown in Fig. 3.5.

3.9 Optimization Algorithm

Nondominated sorting genetic algorithm (NSGA), which is based on a heuristic search algorithm inspired by natural selection theory, is used to solve the optimization problem. NSGA was first proposed by Srinivas and Deb in 1994 for multiobjective problems to find multiple solution points, called Pareto-optimal solutions, instead of trying to find the single solution point [53]. However, NSGA was criticized for 3 main points: 1.) high computational burden of nondominated sorting, 2.) lack of elitism, and 3.) need for sharing parameter specification. Due to these drawbacks, an improved version of NSGA, NSGA-II, was proposed in [54]. NSGA-II has better performance compared to NSGA in terms of obtaining a diverse set of Pareto solutions and better converges to a true Pareto-front set by using a fast nondominating sorting procedure, and preserving the quality of

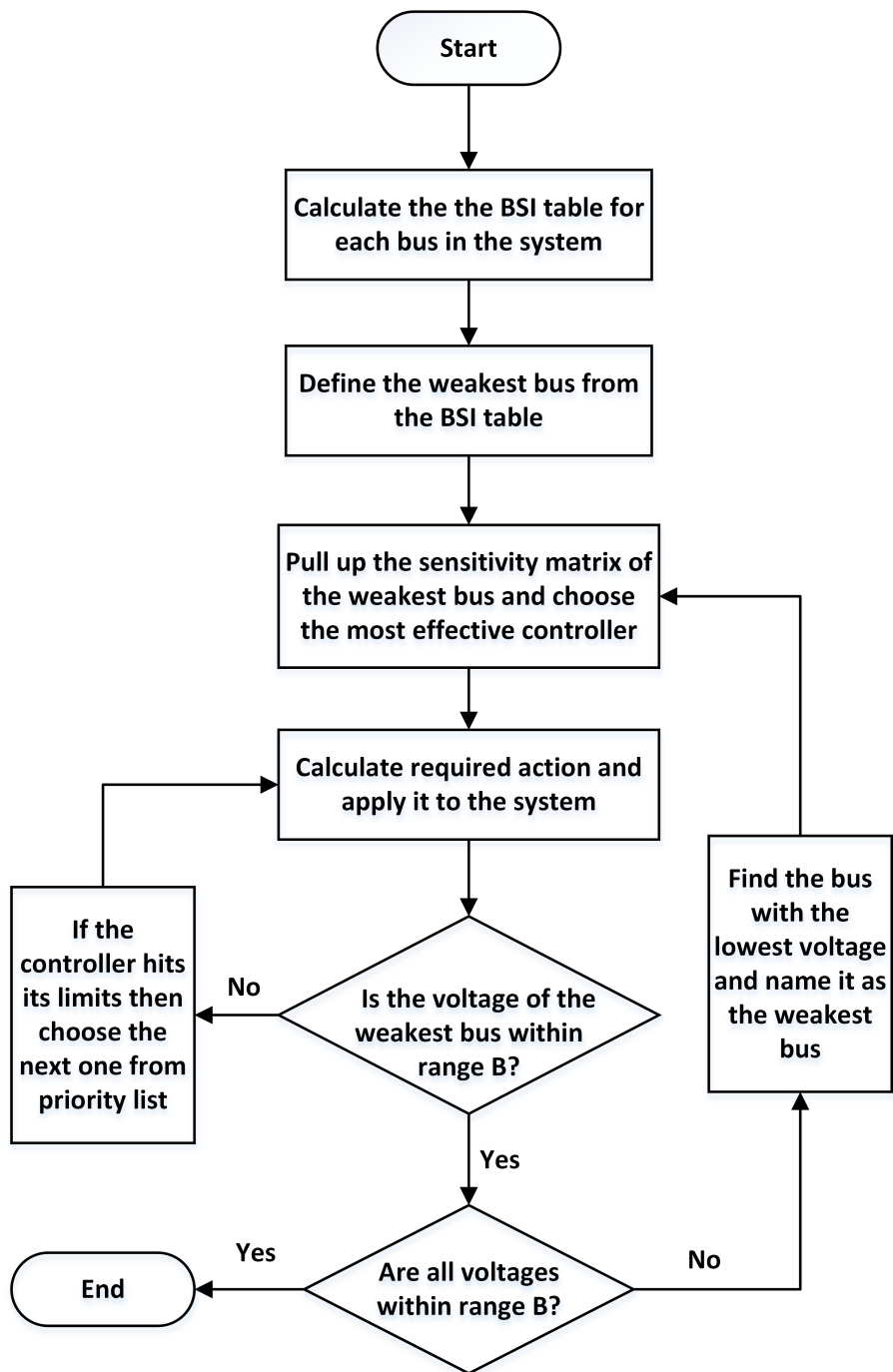


Figure 3.5 Flowchart of the proposed rule-based VVC algorithm

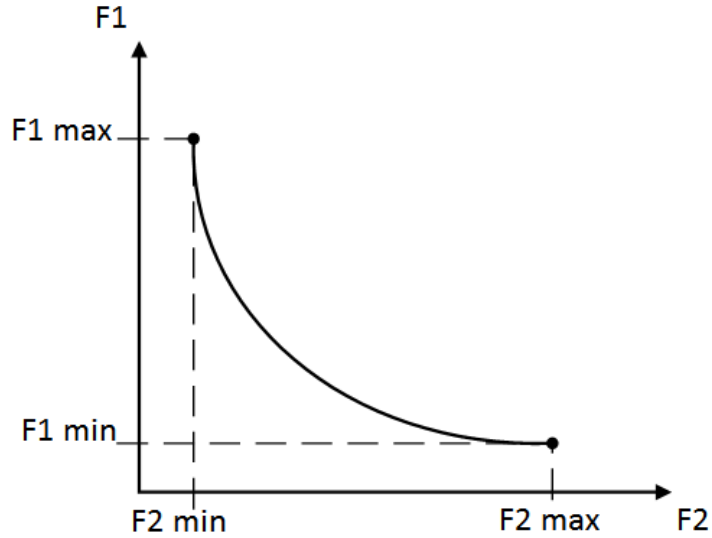


Figure 3.6 Pareto-Front concept of two objective problem solution.

solution. Additionally, it requires $O(MN^2)$ computations in the worst case compared to NSGA which requires $O(MN^3)$ computations where M and N is number of objectives and population size, respectively. Because of the aforementioned improvements, it has been used excessively in the academia for different problems, particularly in power systems related problems, such as in [55, 56].

In NSGA-II, the user does not have to specify any weight for different objectives before the solution. The user chooses his preferred optimal solution from the optimum Pareto front for multiple objectives. In our simulations, we chose the end points of Pareto front, which gives the minimum and maximum available values of each objective function, as shown in Fig. 3.6. The basic operation steps of NSGA-II are as follows:

1. A random parent population (P_t) of size N is created, and is sorted based on the nondomination.

2. Assign a fitness (or rank) to each solution based on its nondomination level.
3. Use binary tournament selection, recombination, and mutation operators to create offspring Q_t population size of N .
4. Form a combined population R_t consisting of parent and offspring population size of $2N$, and sort new population based on the nondomination.
5. Form a new parent population P_{t+1} by using nondominated sets until getting the size of N .
6. Use binary tournament selection, recombination, and mutation operators to create offspring Q_{t+1} population size of N .
7. Use crowding distance sorting to ensure diversity if P_{t+1} is not size of N .
8. Repeat steps 2 to 7 until the stopping criterion is met. The stopping criterion may be the size of population or generation.

For more details, readers are encouraged to refer to reference [54].

3.10 Renewable DG and Load Modelling

This section presents the wind-based renewable DG and load modelling for the system under study.

3.10.1 DG Modelling

Active power output variation of wind turbines is based on the change in wind speed, and it has been shown in the literature that the wind speed profile of a given location can be

represented by a Weibull probability distribution function (pdf) $f_w(v)$ over time [57]. The Weibull pdf equation is given by:

$$f_w(v) = \frac{k}{c} \left(\frac{v}{c}\right)^{k-1} \exp \left[- \left(\frac{v}{c}\right)^k \right], \quad (3.29)$$

where k and c are called shape and scale index, respectively. In order to generate Weibull pdf, the required scale and shape indices can be calculated using standard deviation and average wind speed as follows [58]:

$$k = \left(\frac{\sigma}{\bar{v}}\right)^{-1.086}, \quad c = \frac{\bar{v}}{\Gamma(1 + \frac{1}{k})}, \quad (3.30)$$

where \bar{v} is average wind speed, and $\Gamma()$ is the gamma function.

The forecasting process always has some errors. There are various techniques available in literature for the forecast errors [59–61], but in our study the method proposed in [62] is followed. Therefore, the actual wind speed at a future time t can be expressed as in 3.31:

$$v^a(t) = v^e(t) + \epsilon_w \quad (3.31)$$

where $v^e(t)$ and $v^a(t)$ are expected and actual wind speed for time t , respectively, and ϵ_w is expected wind speed error, which can be modelled by Gaussian distribution with zero means and standard deviation (σ) as $\epsilon_w \sim N(0, \sigma^2)$. The expected value of the error in wind speed could form a confidence interval, as defined in 3.32:

$$\int_{-\alpha \leq \epsilon_w \leq \alpha} f(v, \mu, \sigma) dx = \frac{K}{100}, \quad (3.32)$$

where α is an error margin, and K is a confidence level. Using Eq. (3.32), the expected wind speed interval can be represented as follows:

$$v^e(t) - \alpha \leq v^a(t) \leq v^e(t) + \alpha \quad (3.33)$$

Calculated actual wind speeds can be then converted into wind power data using the wind power curve of the wind turbine generator, as follows [63]:

$$P_{WT}(t) = \begin{cases} 0 & 0 \leq v^a(t) < v_{ci} \\ P_{rated} * \frac{(v^a(t)-v_{ci})}{(v_r-v_{ci})} & v_{ci} \leq v^a(t) < v_r \\ P_{rated} & v_r \leq v^a(t) < v_{co} \\ 0 & v^a(t) \geq v_{co} \end{cases} \quad (3.34)$$

where v_{ci} , v_r , v_{co} are cut-in, rated, and cut-out wind speeds, P_{rated} is the wind turbine rated output power, and $v^a(t)$, $P_{WT}(t)$ are actual wind speed and wind turbine output power at t , respectively.

3.10.2 Load Modelling

The load profile is assumed to follow IEEE-RTS (Institute of Electrical and Electronics Engineers Reliability Test System) hourly load model. This system provides hourly peak load as a percentage of the daily peak load. Four different load profiles are obtained, each representing a typical day in a season, and they are shown in Fig. 3.7 [64, 65].

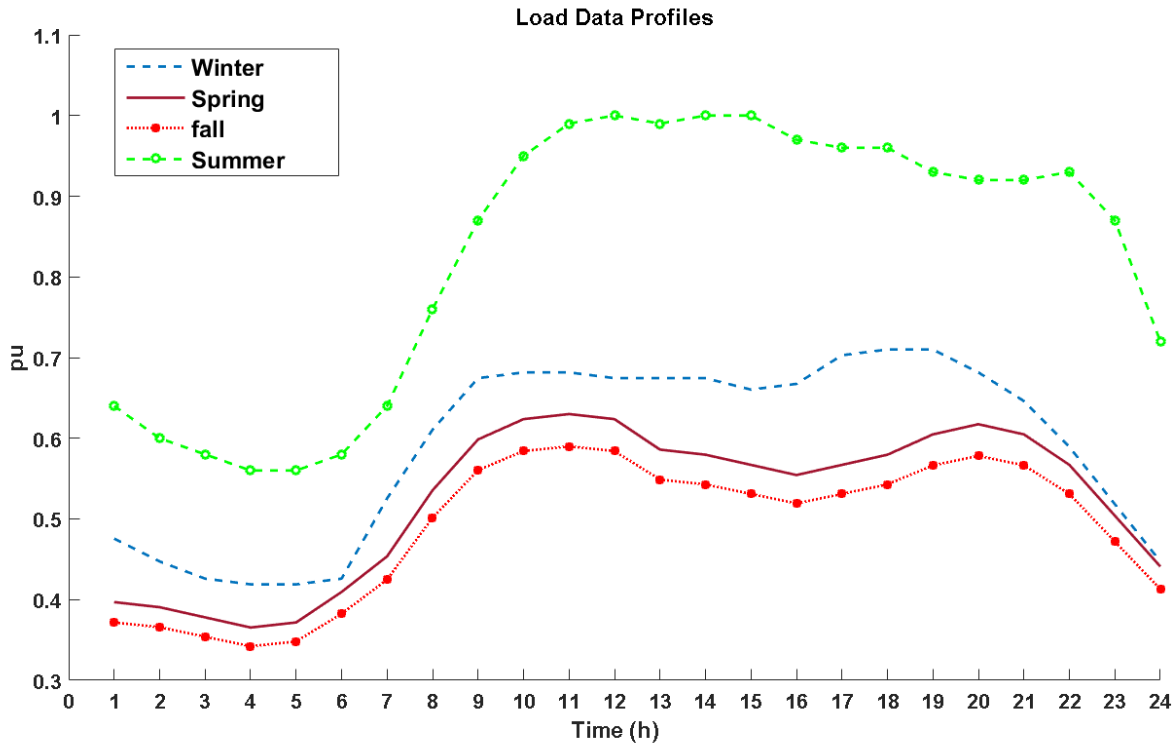


Figure 3.7 Daily load profiles for different seasons.

3.11 Case Studies

This section presents the test systems under study, and the simulation results for different cases; base case, and state A, B, and C cases.

3.11.1 Test Systems

The effectiveness of the proposed approach was tested on IEEE-34 and IEEE-123 bus radial distribution test systems, as shown in Fig. 3.8 and 3.9 [66]. The IEEE-34 bus test system was modified by installing three three-phase renewable wind DGs with 1 MW capacity

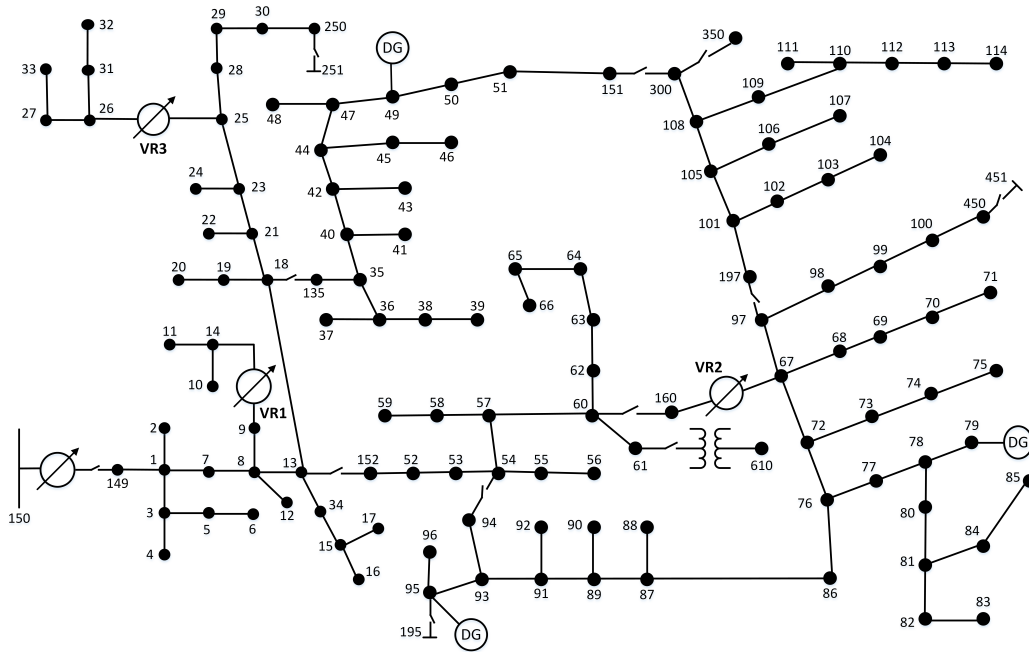


Figure 3.9 One-line diagram of the modified IEEE-123 bus test system.

state identification before each hour to adjust the control strategy accordingly. Historical wind speed data, which was collected from the Bonavista Station of Newfoundland and Labrador, Canada, for seven years (January 1, 1988 to December 31, 1994), is used to generate Weibull pdf for each month to represent randomness in the expected wind speed for each time interval [69]. Day-ahead expected wind speed is assumed to have Gaussian distribution error with zero means and a standard deviation of 2.04. The confidence level (K) is assumed to be 95%, and the speed confidence interval is calculated as 4 using Eq. (3.32) as in Ref. [62]. Then, based on wind speed forecast error intervals, wind power output intervals are calculated using the power curve equation in 3.34. In order to represent the stochastic nature of renewable DG, the expected minimum, mean, and maximum wind speeds are calculated from 50,000 different wind speed scenarios. The expected DG power outputs for a typical day in December is calculated based on expected wind speed and is

shown in the Table 3.1. As a load, the winter load profile has been used for all simulations.

3.11.2.1 Base Case Simulation

As a base case, two different cases have been considered for a day-ahead simulation. First, in base case 1 (BC1), the test systems are assumed to have no control on voltages and controllers, and all regulator taps are assumed at their neutral position. Second, in base case 2 (BC2), the test systems are optimized for loss minimization but no constraint is applied on tap movement limits. All proposed control strategies are tabulated in Table 3.2 in terms of DG involvement and objective types. Daily power losses, total cost, and number of tap changes are calculated for three DG output scenarios: 1.) all DG output powers are at their minimum possible values, 2.) all DG output powers are at their expected values (mean), and 3.) all DG output powers are at their maximum possible values, as shown in Table 3.3 and Table 3.4. It is worth mentioning that, in BC1, the voltages are violating Range A limits, while BC2 has no voltage violation due to the applied control algorithm.

3.11.2.2 State-A simulations

In the state A, the goal of the control strategy is to run the system in the most economical manner by prioritizing inexpensive control devices. The objectives, which are formulated as a multi-objective problem, are the minimization of both daily power loss and daily control cost. The values are reported for daily power loss, control cost, number of total tap switching, curtailed DGs' active power, and total cost in Table 3.3 and 3.4 for IEEE 34 and 123 bus systems, respectively. In Table 3.3 and 3.4, there are two rows for each strategy results; the first row gives the values that are obtained from the right-hand end

point of the Pareto front, which gives the minimum control cost and maximum power loss point for the solution, and the second row represents the values that are obtained from the left-hand side end point of the Pareto front, which gives the minimum power loss and maximum control cost of the Pareto front solution. It can be seen from the Table 3.3 that strategies A1 and A2 reduces the tap movement cost and total cost by decreasing total number of tap movements, while the total daily power losses are increased. There is no DG output power curtailment in strategy A2, and this is due to the low DG penetration level and high price of DG active power curtailment. Also, the results indicates that a DG output power increase results in loss reduction due to less power transfer along the feeders. For the IEEE 123 test system, there is no big difference between BC1, A1 and A2 in terms of loss due to overlapping tap positions for an optimal solution with neutral tap position. It is worth noting that the operational cost is less in BC1 compared to the case of BC2 due to less tap movements.

3.11.2.3 State-B VVC strategies and simulation

For this case, the system is forced to degenerate into state B (*arrow 1*) at hour 5 through the disconnection of the shunt capacitor and the load increase at bus 890. When state B is detected, the voltages at bus 890 are 0.9394, 0.9323 and 0.9365 for phase A, B and C, respectively, and the phase-A voltage of bus 890 is shown in Fig. 3.10.

For multiobjective strategies (Strategy B1 and B2), Table 3.5 reveals that DG involvement increases the power losses by almost 4% and the number of tap switching by 1, but decreases the voltage deviation by 27%. For the single objective case (strategy B3), taking only the voltage deviation as an objective decreases the deviation by 55% as expected, but causes two DGs to be totally curtailed and increases the power loss by 17%, which is not very optimal from a monetary or power loss perspective.

For voltage deviation, a 1 pu voltage reference point has been chosen just to demonstrate that the algorithm can minimize the difference between actual and any desired voltage value.

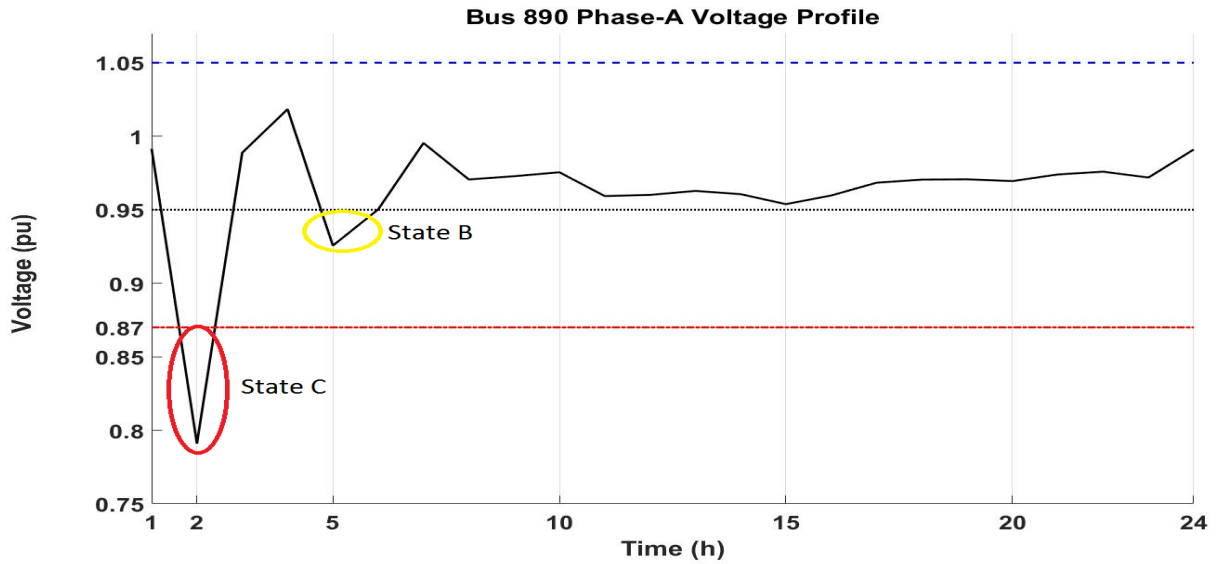


Figure 3.10 Phase-A daily voltage profile of the Bus 890.

3.11.2.4 State-C simulation

In this case, the system is forced to switch into state C by changing the tap positions of regulators to -10 (Table 3.7) and disconnecting the shunt capacitor at bus 890 (*arrow 3*). The voltages before and after the RB algorithm is applied are shown in Table 3.6 of nodes, which have under-voltage violation. The weakest node in the system is identified as phase-A of the bus 890 with a 0.7909 pu voltage, and 0.3969 of BSI, and its voltage profile is shown in Fig. 3.10. As seen in the Table 3.6, after the application of RB control all bus voltages are brought back into state A limits (*arrow 6*) and the all BSIs are increased.

Applying the proposed RB control strategy prevents the system from reaching service interruptions and brings the system back into state B. The control device priority list was used to activate each control device, and only three regulators (namely VR1-a, VR2-a and VR2-c; a and c refer phase a and c) were used to eliminate voltage violation, as in Table 3.7. The RB algorithm decreases the voltage deviation from 0.92 to 0.38, by 58%, but increases the power losses from 70 kW to 80.44 kW, by 15%. No DG power curtailment occurs since their voltage sensitivity values are smaller than the regulators' values.

For states A and B, a genetic algorithm based optimization method takes about 5 minutes to obtain the optimal solution. For state C the number of iterations to get the system back to state-B depends on: 1.) how severe the voltage violation is, in other words, what is the required voltage increase/decrease for the bus/buses with voltage violation to bring their voltage back into state-B, and 2.) the voltage sensitivity indices of the controllers. The proposed rule-based strategy has been repeated for different violation levels many times, and we have observed that the solution time changes from less than a second to a few seconds depending on how severe the voltage violation is and how effective the control devices are.

3.12 Conclusion

This chapter presented the system state index based on the voltage profile, and demonstrated how the transaction scheme operates from one state to another. The bus stability index to identify the weakest bus in the system, and voltage sensitivity analysis of the buses was also provided. Furthermore, cost function of control devices, objective functions, and constraints for the state-based VVC algorithm were presented, and the proposed rule-based emergency state VVC algorithm was discussed.

The simulation results demonstrate that the proposed VVC algorithm operates the system at its optimum, while improving the voltage profile. During the normal operation state, it is found that the DG participation is not a cost-effective option. The results also demonstrated that using DGs as a VVC control device is not always an optimum solution in state B, which may result in monetary loss for the DG owners, especially in the strategies B2 and B3. The proposed rule-based algorithm for the emergency case is very efficient to bring the system back into normal operation conditions in a very short time.

Table 3.1 Forecasted output power (kW) for Wind DG of a typical day in December

Hour	Minimum DG Output	Mean DG Output	Maximum DG Output
1	94.49	115.90	137.90
2	94.66	118.16	140.21
3	99.46	123.69	142.55
4	98.52	120.56	139.41
5	93.86	116.93	139.41
6	92.95	118.58	136.18
7	100.83	123.79	139.82
8	94.02	119.41	138.28
9	91.31	113.08	131.65
10	91.64	114.83	132.95
11	90.54	114.31	132.69
12	76.29	98.28	122.27
13	74.09	101.46	122.20
14	76.86	98.71	122.80
15	80.13	104.57	127.85
16	94.28	117.74	137.05
17	95.42	122.01	143.75
18	99.15	122.63	144.26
19	83.90	105.26	122.93
20	95.11	119.73	132.90
21	93.04	116.60	133.09
22	93.65	119.94	138.61
23	84.87	109.81	128.97
24	96.12	119.61	142.13

Table 3.2 Control Strategies and Corresponding DG Involvements and Objective Types

Strategy Type	DG Involvement		Objective Type	
	Yes	No	Single	Multi
BC2		✓	✓	
A1		✓		✓
A2	✓			✓
B1		✓		✓
B2	✓			✓
B3	✓		✓	
C	✓		✓	

Table 3.3 State A Control Strategies with Corresponding Daily Control Devices States and Objective Function Values for IEEE 34 Bus System

Strategy Type	# of N_{Tap}	Curtailed $P_{DG}(kW)$	$P_{loss}(MW)$	C_{Cost} (\$/Day)	Total Cost (\$/Day)
BC1 DG_{min}	0	0	1.7680	0	226.30
BC1 DG_{mean}	0	0	1.6048	0	205.41
BC1 DG_{max}	0	0	1.4920	0	190.97
BC2 DG_{min}	124	0	1.648	173.6	384.54
BC2 DG_{mean}	116	0	1.444	162.4	347.23
BC2 DG_{max}	124	0	1.325	173.6	343.2
A1 DG_{min}	57	0	1.7384	79.8	302.31
	58	0	1.7379	81.2	303.65
A1 DG_{mean}	51	0	1.5512	71.4	269.95
	-	-	-	-	-
A1 DG_{max}	58	0	1.4594	81.2	268
	-	-	-	-	-
A2 DG_{min}	34	0	1.8230	47.6	280.94
	-	-	-	-	-
A2 DG_{mean}	51	0	1.5587	71.4	270.91
	-	-	-	-	-
A2 DG_{max}	58	0	1.4521	81.2	267
	60	0	1.4516	84	269.80

Table 3.4 State A Control Strategies with Corresponding Daily Control Devices States and Objective Function Values for IEEE 123 Bus System

Strategy Type	# of N_{Tap}	Curtailed $P_{DG}(kW)$	$P_{loss}(kW)$	C_{Cost} (\$/Day)	Total Cost (\$/Day)
BC1 DG_{min}	0	0	508.56	0	65.09
BC1 DG_{mean}	0	0	444.47	0	56.89
BC1 DG_{max}	0	0	405.84	0	51.94
BC2 DG_{min}	122	0	495.37	170.8	234.2
BC2 DG_{mean}	137	0	436.45	191.8	247.66
BC2 DG_{max}	137	0	394.7	191.8	242.32
A1 DG_{min}	2	0	509.23	2.8	67.98
	63	0	505.50	88.2	152.9
A1 DG_{mean}	4	0	445.50	5.6	62.62
	20	0	444.14	28	84.84
A1 DG_{max}	4	0	405.00	5.6	57.44
	13	0	403.33	18.2	69.82
A2 DG_{min}	0	0	511.25	0	65.44
	-	-	-	-	-
A2 DG_{mean}	0	0	444.94	0	56.95
	9	0	444.17	12.6	69.45
A2 DG_{max}	0	0	404.50	0	51.77
	10	1.85	403.75	14	65.91

Table 3.5 State B Control Strategies with Corresponding Control Device States and Objective Function Values

Strategy Type	Number of N_{Tap}	Curtailed $P_{DG}(kW)$	$P_{loss}(kW)$	Voltage Deviation (V_D)	Total Cost (\$/hour)
B1	5	0	84.1	0.10	17.76
B2	6	1.14	87	0.073	19.68
B3	5	125	101.9	0.0045	36.04

Table 3.6 Bus Voltages and BSIs pre- and post-Emergency State Control Actions

Node	pre-V (pu)	post-V (pu)	pre-BSI	post-BSI
832.1	0.8622	1.0571	0.4546	1.0355
858.1	0.8612	1.0561	0.4541	1.0344
834.1	0.8600	1.0550	0.4519	1.0307
860.1	0.8598	1.0548	0.4500	1.0278
842.1	0.8600	1.0550	0.4500	1.0280
836.1	0.8596	1.0547	0.4495	1.0270
840.1	0.8596	1.0547	0.4493	1.0266
862.1	0.8596	1.0547	0.4493	1.0266
844.1	0.8600	1.0550	0.4499	1.0277
846.1	0.8601	1.0553	0.4498	1.0276
848.1	0.8602	1.0553	0.4503	1.0291
864.1	0.8612	1.0561	0.4524	1.0320
890.1	0.7909	0.9909	0.3969	0.9349
890.2	0.8095	0.9040	0.4272	0.4406
890.3	0.8096	0.9599	0.4343	0.8160

Table 3.7 State C Rule-Based Control Strategy with Corresponding Control Device States and Objective Function Values

RB Algorithm	Tap Positions	Curtailed P_{DG} (kW)	P_{loss} (kW)	Voltage Deviation V_D
Not Applied	[-10 -10 -10 -10 -10 -10]	0	70	0.92
Applied	[8 -10 -10 4 -10 13]	0	80.44	0.38

Chapter 4

Zone-Oriented Distributed Convex VVC Algorithm

4.1 Introduction

In this chapter, different system component models are provided, and an overview of positive semidefinite formulation of power flow equations is presented. Then, we provide a chordal relaxation based formulation of the VVC problem. Next, the proposed clustering method and hierarchical distributed zone-oriented convex VVC problem are defined and a solution algorithm is provided. Lastly, simulation results, and conclusions are presented.

4.2 System Modelling

In this section, we present system components for convex optimal power flow (OPF) problem formulation. An h bus distribution network that includes k VRs can be equiv-

alently represented as $(h + k)$ bus distribution network including k number of virtual secondary side buses for VRs. The edge-set that represents the distribution lines is $\varepsilon := \{(n, m) | n, m \in N\} \subseteq N \times N$, where N is the set of total buses $\{1, \dots, h, h + 1, \dots, k\}$. Three-phase system admittance matrix $Y \in \mathbb{C}^{3(h+k) \times 3(h+k)}$ could be represented based on system topology. Each 3x3 block sub-matrices of Y matrix can be formed as follows:

$$Y_{nm} = \begin{cases} \sum_{m:(n,m)} y_{nm}, & \text{if } n = m, \\ -y_{nm}, & \text{if } n \neq m \text{ and } (n, m), \\ 0, & \text{No connection between bus } n \text{ and } m, \end{cases} \quad (4.1)$$

where, y_{nm} is a 3x3 block phase admittance matrix representing the line between bus n and m which is given as follows:

$$y_{nm} := \begin{bmatrix} y_{nm}^{a,a} & y_{nm}^{a,b} & y_{nm}^{a,c} \\ y_{nm}^{b,a} & y_{nm}^{b,b} & y_{nm}^{b,c} \\ y_{nm}^{c,a} & y_{nm}^{c,b} & y_{nm}^{c,c} \end{bmatrix} \quad (4.2)$$

An admittance element representing phase ϕ of bus n with phase ρ of bus m is shown as $y_{nm}^{\phi,\rho}$. It would have zeros for each entry representing missing phases for single- and two-phase lines. For example, a two-phase line admittance matrix, phase a and b , would

be as follows:

$$y_{nm} := \begin{bmatrix} y_{nm}^{a,a} & y_{nm}^{a,b} & 0 \\ y_{nm}^{b,a} & y_{nm}^{b,b} & 0 \\ 0 & 0 & 0 \end{bmatrix} \quad (4.3)$$

Let voltage of phase ϕ of bus n is defined as $V_n^\phi = |V_n^\phi| \angle \theta_n^\phi$, then the corresponding complex voltage vector of the system can be defined as $V = [V_1^a \ V_1^b \ V_1^c \ \dots \ V_{h+k}^a \ V_{h+k}^b \ V_{h+k}^c]^T$.

4.2.1 Renewable Energy Resources (RESs) Modelling

Renewable energy resources are assumed to be connected to the system via an inverter with a given complex power capacity. RES owners usually sell their excess energy to utility companies, and their earnings are given via a linear function as follows:

$$C_g(P_{DG}) = \sum_{\phi \in \psi_{DG}} c_e \cdot [(1 - \eta_{DG}) \cdot P_{DG}^\phi], \quad (4.4)$$

where c_e is contract energy price for RES's output power, η_{DG} is the loss factor of the inverter, P_{DG}^ϕ is the active power generation of RES at phase ϕ , and ψ_{DG} is the phase set of the RES bus.

RESs also have limits on their active/reactive power injection as given in (4.5); the active power is also limited by power factor, and inverter capacity as shown in (4.6), and (4.7), respectively:

$$P_{DG}^{\min} \leq P_{DG}^\phi \leq P_{DG}^{\max}; \quad Q_{DG}^{\min} \leq Q_{DG}^\phi \leq Q_{DG}^{\max}, \quad (4.5)$$

$$\frac{PF_{DG}^{\min}}{\sqrt{1 - (PF_{DG}^{\min})^2}} Q_{DG}^{\phi} \leq P_{DG}^{\phi} \leq \frac{PF_{DG}^{\max}}{\sqrt{1 - (PF_{DG}^{\max})^2}} Q_{DG}^{\phi}, \quad (4.6)$$

$$(P_{DG}^{\phi})^2 + (Q_{DG}^{\phi})^2 \leq (S_{DG}^{\phi, \max})^2, \quad (4.7)$$

where P_{DG}^{ϕ} and Q_{DG}^{ϕ} are active/reactive power for phase ϕ . $S_{DG}^{\phi, \max}$ represents the maximum apparent power capacity of the inverter for phase ϕ , and PF_{DG} represents the power factor.

4.2.2 Load Modelling

Constant loads are considered, and load at phase ϕ of bus n is modelled as constant real and reactive power demands, $P_{n,d}^{\phi}$, and $Q_{n,d}^{\phi}$, respectively.

4.2.3 Capacitor Bank Modelling

Capacitor banks can adjust their reactive power supply within their allowed ranges, as in (4.8):

$$Q_s^{\min} \leq Q_{s,q}^{\phi} \leq Q_s^{\max}, \quad s \in C_s, \phi \in \psi_s, \quad (4.8)$$

where $Q_{s,q}^{\phi}$ is the reactive power injection of phase ϕ of capacitor s , and C_s and ψ_s are the set of shunt capacitor and set of phases of capacitor s , respectively.

4.2.4 Voltage Regulator Modelling

A voltage regulator (VR) is modeled as an ideal transformer with a primary side connected to bus n and a virtual secondary side connected to bus m , as shown in Fig. 4.1 [70]. The relationship between primary and virtual secondary bus voltages and the tap ratio limits

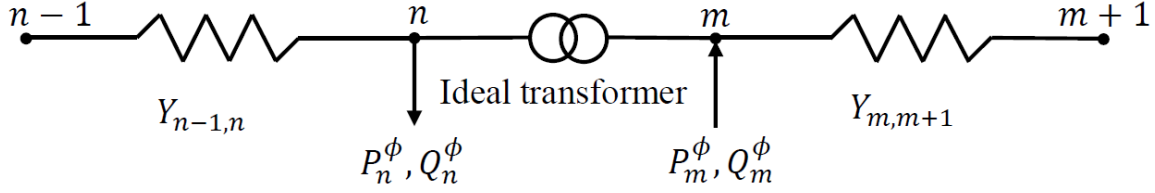


Figure 4.1 Equivalent circuit of VR transformer

are given in (4.9a), and the active and reactive power relations are stated in (4.9b):

$$T_{n,m}^\phi \cdot V_n^\phi = V_m^\phi, \quad T_{n,m}^{\min} \leq T_{n,m}^\phi \leq T_{n,m}^{\max}, \quad (4.9a)$$

$$P_n^\phi = P_m^\phi; \quad Q_n^\phi = Q_m^\phi, \quad (n, m) \in K. \quad (4.9b)$$

where V_n^ϕ , and V_m^ϕ are complex voltage at phase ϕ of buses n and m , respectively. $T_{n,m}^\phi$ is the tap ratio of phase ϕ of VR between bus n and m , while P_n^ϕ/Q_n^ϕ and P_m^ϕ/Q_m^ϕ are the active/reactive power injection of phase ϕ from bus n and bus m , respectively. K represents the set of VRs in the system.

4.3 Convex Volt/Var Control Problem Formulation

A bus in a power systems can have only a generator, only a load, both of them or neither of them connected to it. Complex power injection (generation minus load) to the system from phase ϕ of bus n is given in (4.10a), and it can also be represented via compact matrix form as in (4.10b). Both active and reactive power can also be represented in compact form as in (4.10c). Furthermore, the $\Phi_{P,n}^\phi$ and $\Phi_{Q,n}^\phi$ matrices are defined in (4.10d), while

Y_n^ϕ is given in (4.10e).

$$S_n^\phi = V_n^\phi \cdot \left(\sum_{\rho \in \psi_n} Y_{n,n}^{\phi,\rho} \cdot V_n^\rho + \sum_{m \in \Omega_n} \sum_{\rho \in \psi_n} Y_{n,m}^{\phi,\rho} \cdot V_m^\rho \right)^* \quad (4.10a)$$

$$S_n^\phi = \text{tr}(\Phi_{P,n}^\phi \cdot V \cdot V^H) + j \cdot \text{tr}(\Phi_{Q,n}^\phi \cdot V \cdot V^H) \quad (4.10b)$$

$$P_n^\phi = \text{tr}(\Phi_{P,n}^\phi \cdot V \cdot V^H); \quad Q_n^\phi = j \cdot \text{tr}(\Phi_{Q,n}^\phi \cdot V \cdot V^H) \quad (4.10c)$$

$$\Phi_{P,n}^\phi = \frac{1}{2}(Y_n^\phi + (Y_n^\phi)^H); \quad \Phi_{Q,n}^\phi = \frac{j}{2}(Y_n^\phi - (Y_n^\phi)^H) \quad (4.10d)$$

$$Y_n^\phi = e_n^\phi \cdot (e_n^\phi)^T \cdot Y \quad (4.10e)$$

where e_n^ϕ is the $3 \times N$ -dimensional Kronecker vector of zeros, except for the $(3n + \phi)^{th}$ entry, which is equal to 1, where $\phi = 1, 2$, and 3 represent phases a, b , and c , respectively.

We can define a positive semidefinite matrix variable $W \in \mathbb{C}^{3 \times N, 3 \times N}$ as the outer product of complex voltage vector V as follows:

$$W = V \cdot V^H = \begin{bmatrix} V_0 \\ \vdots \\ V_N \end{bmatrix} \begin{bmatrix} V_0^H \\ \vdots \\ V_N^H \end{bmatrix} = \begin{bmatrix} |V_1^a|^2 & (V_1^a)(V_1^b)^* & (V_1^a)(V_1^c)^* & (V_1^a)(V_2^a)^* & \cdots & (V_1^a)(V_N^c)^* \\ (V_1^b)(V_1^a)^* & |V_1^b|^2 & (V_1^b)(V_1^c)^* & (V_1^b)(V_2^a)^* & \cdots & (V_1^b)(V_N^c)^* \\ \vdots & \vdots & \ddots & \vdots & & \\ (V_N^c)(V_1^a)^* & (V_N^c)(V_1^b)^* & (V_N^c)(V_1^c)^* & (V_N^c)(V_2^a)^* & \cdots & |V_N^c|^2 \end{bmatrix}$$

The power equations in (4.10) are linearly related to the entries of W ; therefore, one can formulate an optimal power flow problem in semidefinite programming form (SDP-OPF)

as follows:

$$\min_W f(W) \tag{4.11a}$$

$$p_n^{min} \leq tr(\Phi_{P,n}^\phi W) \leq p_n^{max}, \quad \forall n \in Ng, \phi \in \psi_n \tag{4.11b}$$

$$q_n^{min} \leq tr(\Phi_{Q,n}^\phi W) \leq q_n^{max}, \quad \forall n \in Ng, \phi \in \psi_n \tag{4.11c}$$

$$(v_n^{min})^2 \leq tr(E_n^\phi W) \leq (v_n^{max})^2, \quad \forall n \in N, \phi \in \psi_n \tag{4.11d}$$

$$tr(\Phi_{P,n}^\phi W) = \sum_{g \in N_g} P_{n,g}^\phi - \sum_{d \in Nl} P_{n,d}^\phi + \Lambda_n \cdot P_n^\phi \tag{4.11e}$$

$$tr(\Phi_{Q,n}^\phi W) = \sum_{g \in N_g} Q_{n,g}^\phi - \sum_{d \in Nl} Q_{n,d}^\phi + \sum_{q \in C_s} Q_{n,q}^\phi + \Lambda_n \cdot Q_n^\phi \tag{4.11f}$$

$$T_{n,m}^2 \cdot W_{n,n} = W_{m,m}, \quad \forall (n, m) \in K \tag{4.11g}$$

$$T_{n,m}^{min} \leq T_{n,m}^\phi \leq T_{n,m}^{max}, \quad \phi \in \psi_{n,m} \tag{4.11h}$$

$$[V_0^a, V_0^b, V_0^c]^T = \hat{V}_0 \tag{4.11i}$$

$$W \succeq 0, \quad rank(W) = 1 \tag{4.11j}$$

$$\text{s.t. } (4.5), (4.6), (4.7), (4.8), (4.9b). \tag{4.11k}$$

where $E_n^\phi = e_n^\phi \cdot (e_n^\phi)^T$. For SDP-OPF if the optimal solution matrix W^* has rank-1, then an optimal solution V^* is recovered through the unique spectral decomposition of $W^* = V^* \cdot (V^*)^H$.

In problem (4.11), constraints (4.11b) and (4.11c) represent the active and reactive power generation limits, respectively, while constraint (4.11d) sets the upper and lower boundaries for bus voltages. Bus active and reactive power injection equations are given in (4.11e) and (4.11f), respectively. The constraint (4.11g) defines VR voltage relation that can be written more explicitly as in (4.12) and (4.13). Equality constraint (4.11i) defines the given substation bus voltage, and Λ_n is defined to represent the connection topology

of VR and substation bus as given in (4.14).

$$T_{n,m}^2 \cdot (V_n V_n^H) = V_m V_m^H \Rightarrow T_{n,m}^2 \cdot W_{n,n} = W_{m,m} \quad (4.12)$$

$$T_{n,m}^2 \cdot \begin{bmatrix} W_{n,n}^{a,a} & W_{n,n}^{a,b} & W_{n,n}^{a,c} \\ W_{n,n}^{b,a} & W_{n,n}^{b,b} & W_{n,n}^{b,c} \\ W_{n,n}^{c,a} & W_{n,n}^{c,b} & W_{n,n}^{c,c} \end{bmatrix} = \begin{bmatrix} W_{m,m}^{a,a} & W_{m,m}^{a,b} & W_{m,m}^{a,c} \\ W_{m,m}^{b,a} & W_{m,m}^{b,b} & W_{m,m}^{b,c} \\ W_{m,m}^{c,a} & W_{m,m}^{c,b} & W_{m,m}^{c,c} \end{bmatrix} \quad (4.13)$$

$$\Lambda_n = \begin{cases} -1 & \text{if } (n, m) \in K \\ 1 & \text{if } (m, n) \in K \text{ or } n = 0 \\ 0 & \text{otherwise} \end{cases} \quad (4.14)$$

The problem (4.11) is still nonconvex due to the VR voltage equality constraint (4.11g) and rank constraint of (4.11j). However, the problem can be relaxed to a convex one by dropping the rank-1 constraint on W , and replacing the VR voltage equality constraint by relaxed inequalities of (4.15) for continuous VR tap ratio modelling [71]:

$$(T_{n,m}^{max})^2 \cdot W_{n,n} - W_{m,m} \succeq 0 \quad (4.15a)$$

$$-(T_{n,m}^{min})^2 \cdot W_{n,n} + W_{m,m} \succeq 0 \quad (4.15b)$$

On the other hand, for discrete VR tap ratio modelling, VR tap constraint (4.11g) is

replaced by the relaxed inequality constraints of (4.16) to obtain convex problem [71].

$$W_{m,m} = \left[\sum_{k=0}^{2T_t} (T_{n,m}^{min} + C_{n,m} \cdot k)^2 \cdot T_{n,m}^k \right] \cdot W_{n,n} \quad (4.16a)$$

$$\sum_{t=0}^{2T_t} T_{n,m}^k = 1, \quad T_{n,m}^k \in (0, 1) \quad (4.16b)$$

$$-M \cdot T_{n,m}^k \leq W_{n,m,k}^{\phi,\rho} \leq M \cdot T_{n,m}^k \quad (4.16c)$$

$$W_{n,n}^{\phi,\rho} - (1 - T_{n,m}^k) \cdot M \leq W_{n,m,k}^{\phi,\rho} \leq W_{n,n}^{\phi,\rho} + (1 - T_{n,m}^k) \cdot M \quad (4.16d)$$

where, $T_{n,m}^k$ is the discrete tap ratio indicator, and it can only take certain values that are governed by $T_{n,m}^k = T_{n,m}^{min} + C_{n,m} \cdot k$ expression for $0 \leq k \leq 2T_t$, where, $2T_t$ is the total available discrete tap positions. $W_{n,m,k}^{\phi,\rho}$ is the auxiliary variable to substitute the nonconvex multiplication term of $T_{n,m}^k \cdot W_{n,n}^{\phi,\rho}$, and M is a complex constant of $M = [(1 + j) \cdot abs(V_n^\phi)^{max} \cdot abs(V_m^\rho)^{max}]$. The step size of discrete tap ratio, $C_{n,m}$, is calculated as follows:

$$C_{n,m} = (T_{n,m}^{max} - T_{n,m}^{min}) / 2T_t. \quad (4.17)$$

4.3.1 Chordal Relaxation Based VVC Model for Multiphase Radial Distribution Networks

Consider a graph $G = (N, \varepsilon)$ with vertex set $N := (1, \dots, h + k)$ and edge set $\varepsilon := \{(a, b), (b, c), \dots, (i, j)\}$. Two nodes are called *adjacent* if they are connected to each other and denoted as $(i, j) \in \varepsilon$. A graph is called *complete graph* if every pair of nodes is adjacent. A *subgraph* of G is defined as $F = (N', \varepsilon')$ with $N' \subseteq N$ and $\varepsilon' \subseteq \varepsilon$. A *clique* of G is a complete subgraph of G and a *maximal clique* of G is a clique that is not a subgraph of another clique of G . A *walk* in a graph G is an alternating order of nodes and edges,

and a *trail* is a walk of no edge repetition. A *path* in a graph is a trail such that no node is repeated. If a path starting and end vertex are the same node that it is called a *cycle*, and a cycle is called a *minimal cycle* if it has no *chord* (an edge connecting two vertexes that are not adjacent). A graph is a *chordal graph* if all its minimal cycles have at most 3 nodes. In graph theory, a k -node complete subgraph that has the property of having every node is connected with $(k-1)$ nodes is defined as a *k -clique*. If a k -clique is not contained by any other higher order clique, it is called a *maximal k -clique*. We can model the power systems by using maximal cliques such as 6, 4, and 2-cliques representing three-, two-, and one-phase lines, respectively.

For the SDP-OPF formulation in (4.11), the system voltage outer product is represented by a single square matrix of W of size of $3N \times 3N$ that makes it computationally hard to solve, especially for large distribution networks. However, recently various relaxation techniques have been proposed recently for multiphase radial distribution systems to tackle this computational challenge via exploiting the tree structure of the networks [72, 73]. In these works, the whole network variable matrix (W) is divided into smaller square sub-matrices (W_s) for each maximal clique in the chordal graph; practically, each distribution line is represented by one sub-matrix of W_s . Further detail of sub-matrices construction is provided in Appendix A.

For a given two bus system (bus i and j) the corresponding principal submatrix of $W_s(i, j)$ can be given by:

$$W_s(i, j) := \begin{bmatrix} w_{ii} & w_{ij} \\ w_{ji} & w_{jj} \end{bmatrix}, \quad (i, j) \in \varepsilon \quad (4.18)$$

where, $w_{ii} = V_i \cdot V_i^H$, $w_{jj} = V_j \cdot V_j^H$, $w_{ij} = V_i \cdot V_j^H$, and $w_{ji} = V_j \cdot V_i^H$. The size of each submatrix $W_s(i, j)$ will be 6×6 , 4×4 , or 2×2 for corresponding 3, 2, and 1-phase distribution lines, respectively. The SDP-OPF problem of (4.11) can be rewritten as a chordal relaxed SDP-VVC for continuous tap ratio variables as follows:

$$\min_{\substack{W_s, P_{DG}, Q_{DG}, \\ T_{n,m}, C_g}} f(W) + \sum_{g \in N_g} C_g \quad (4.19a)$$

$$p_n^{min} \leq \text{tr}(\Phi_{P,n}^\phi W) \leq p_n^{max}, \quad \forall n \in Ng, \phi \in \psi_n \quad (4.19b)$$

$$q_n^{min} \leq \text{tr}(\Phi_{Q,n}^\phi W) \leq q_n^{max}, \quad \forall n \in Ng, \phi \in \psi_n \quad (4.19c)$$

$$v_n^{min} \leq \text{tr}(E_n^\phi W) \leq v_n^{max}, \quad \forall n \in N, \phi \in \psi_n \quad (4.19d)$$

$$\text{tr}(\Phi_{P,n}^\phi W) = \sum_{g \in Ng} P_{n,g}^\phi - \sum_{d \in Nl} P_{n,d}^\phi + \Lambda_n \cdot P_n^\phi \quad (4.19e)$$

$$\text{tr}(\Phi_{Q,n}^\phi W) = \sum_{g \in Ng} Q_{n,g}^\phi - \sum_{d \in Nl} Q_{n,d}^\phi + \sum_{q \in C_s} Q_{n,q}^\phi + \Lambda_n \cdot Q_n^\phi \quad (4.19f)$$

$$T_{n,m}^{min} \leq T_{n,m}^\phi \leq T_{n,m}^{max}, \quad \phi \in \psi_{n,m} \quad (4.19g)$$

$$C_g = c_e^\phi \cdot [(1 + n_{DG}) \cdot P_{DG}^\phi], \quad \phi \in \psi_g \quad (4.19h)$$

$$W_s \succeq 0; \quad \forall s \in S \quad (4.19i)$$

$$\begin{bmatrix} (S_{DG}^{max})^2 & P_{DG} & Q_{DG} \\ P_{DG} & 1 & 0 \\ Q_{DG} & 0 & 1 \end{bmatrix} \succeq 0 \quad (4.19j)$$

$$\text{s.t. } (4.5), (4.6), (4.8), (4.9b), (4.15), (4.16). \quad (4.19k)$$

Equation (4.19j) is the Schur complement of nonconvex inverter capacity limit in (4.7). If all sub-matrices are corresponding and all minimal cliques in the system are PSD and

rank-1, then one can construct the full square matrix of W that is the optimal solution of the system.

4.3.2 Objective Functions

The objective function $f(W)$ is targeted at the minimization of three factors: power loss, voltage deviation, and tap movement. Each objective function will be presented in details in the following subsections.

4.3.2.1 Minimization of Power Loss

The active power flow from bus i to bus j over line $(i, j) \in \varepsilon$ is given by $P_{ij} := \text{Re}(\sum_{\phi \in \psi_i} V_i^\phi (I_{ij}^\phi)^*)$, where I_{ij}^ϕ is the complex current flow from bus i to j on phase ϕ , V_i^ϕ is the complex voltage at phase ϕ of bus i , ψ_i is the set of phases of bus i , and ε is the set of lines. Therefore, the power loss minimization can be expressed as follows:

$$P_{loss} = \sum_{(i,j) \in \varepsilon} (P_{ij} + P_{ji}), \quad (4.20)$$

where P_{ji} is the total active power flow from bus j to bus i .

To formulate the power flow in a convex form, let us define $A_{ij} := -e_j^T Y^H e_i E_{ij}$, where $E_{ij} := (e_i - e_j)e_i^T$, then the complex power flowing from bus i to bus j over line $(i, j) \in \varepsilon$ is defined as follows [70]:

$$S_{ij} = \text{tr}(A_{ij}W) = \text{Re}(\text{tr}(A_{ij}W)) + \text{Im}(\text{tr}(A_{ij}W)), \quad (4.21)$$

The objective of minimizing active power losses in the distribution system for a specific

time period of T can now be formulated in a convex form as follows:

$$f_0(W) = w_0 \sum_{t=1}^T \sum_{(i,j) \in \varepsilon} \left[\text{Re}(\text{tr}(A_{ij}W)) + \text{Re}(\text{tr}(A_{ji}W)) \right], \quad (4.22)$$

where w_0 is the weight coefficient of the objective function.

4.3.2.2 Minimization of Voltage Deviation

The objective function of minimizing the voltage deviation from a reference value can be formulated as follows:

$$f_1(W) = w_1 \sum_{t=1}^T \sum_{i \in N} \left((V_{i,t}^{set})^2 - [W^t]_{ii} \right)^2, \quad (4.23)$$

where $[W^t]_{ii}$ is the square of voltage V_i at time t , w_1 is a positive weighting factor, $V_{i,t}^{set}$ is the voltage reference value of bus i at time t , and N is the set of buses.

4.3.2.3 Minimization of the VR Tap Movement

In general, control algorithms that are proposed for minimizing active power losses increase operational costs due to excessive tap movements that are undesirable from a monetary point of view. Therefore, to obtain a global optimal monetary solution, we aim to minimize the VR tap movements, that is:

$$f_2(\text{tap}) = w_2 \sum_{t=1}^T \sum_{i \in K} (\text{tap}_i^{t+1} - \text{tap}_i^t)^2, \quad (4.24)$$

where w_2 is the objective function weight coefficient, tap_i^t is the tap position of i^{th} VR at time t , and K is the set of VRs.

4.4 Hierarchical Distributed Zone-Oriented 2-Stage VVC Strategy

Distribution systems may have various types of electricity consumers, such as residential, industrial, or commercial electricity users. Each consumer type has different priorities, characteristics and requirements. For example, the voltage magnitude deviation, which can deteriorate the life expectancy of electrical equipment, is not a top priority for residential consumers, but achieving a minimum bill is a priority. On the other hand, for industrial and commercial consumers who may have power equipment or manufacturing processes that are sensitive to voltage level, receiving a constant voltage level can be their top priority in order to prevent such issues as a loss of production, equipment damage, and economical losses.

Therefore, treating each customer alike may yield non-optimal results for different customer types. Based on this argument, we proposed a novel zone-based VVC algorithm in which we developed a clustering technique to divide the system into sub-networks based on the consumer type, such as residential, industrial, or commercial zones. Optimization problem parameters will be adjusted according to each zone's needs, which will increase the customer satisfaction level. Each zone has a power loss minimization objective, which is required to have rank-1 solution matrix and some additional zone-specific objectives as shown in Table 4.1. It is noteworthy to mention that different objectives can be added to the zones, depending on the specific zone needs.

Table 4.1 Zone-based Control Strategies and Objective Types

Objective Type	Residential Zone	Industrial Zone	Commercial Zone
Power Loss, $f_0(W)$	✓	✓	✓
Voltage deviation, $f_1(W)$		✓	✓
Tap movement, $f_2(W)$	✓		

4.4.1 System Clustering and Hierarchical Distributed Solution Algorithm

In this subsection, zone clustering and the proposed hierarchical distributed solution algorithm will be explained in more detail.

4.4.1.1 System Clustering

For a given n bus radial distribution system, we divide the network into a number of zones based on the customer types. An example is illustrated in Fig 4.2. The zones set is defined as $c = \{1, 2, \dots, z\}$, where z is the total number of zones in the system. Zone 1 denotes the zone which contains the point of common connection (PCC), and Zone z denotes the furthest zone which has the most number of upstream zones between itself and Zone 1. To maintain solution connectivity between neighbouring zones, an extended zone is formed for each zone in the network according to formulation in (4.25):

$$\hat{c}_i = \begin{cases} c_i & \text{if } i = 1, \\ c_i + Cbus_i & \text{if } i \neq 1, \quad \forall i \in c, \end{cases} \quad (4.25)$$

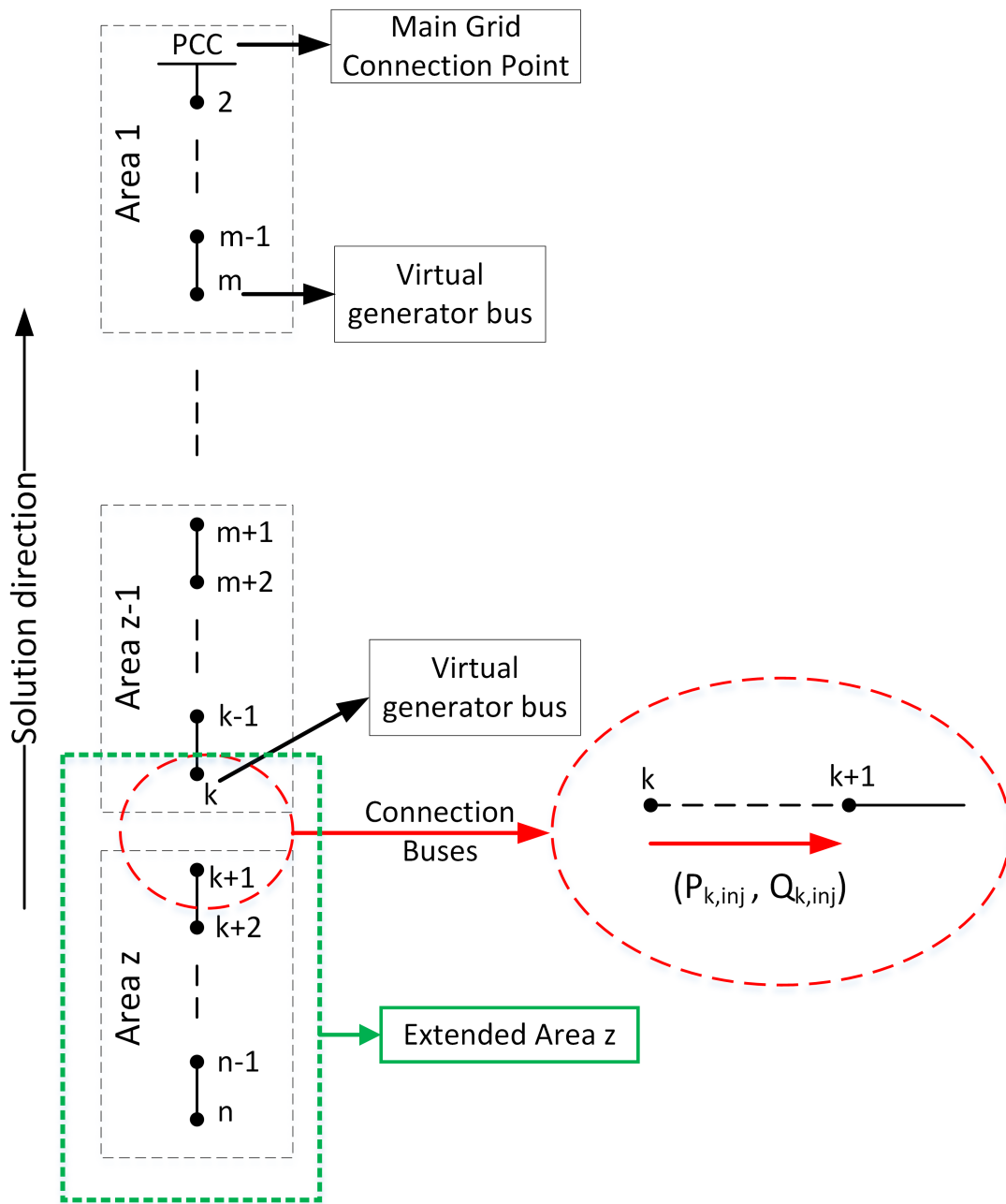


Figure 4.2 Flowchart of the proposed hierarchical distributed algorithm.

where c_i is the bus set of zone i . Any given extended zone \hat{c}_i contains connection buses ($Cbus_i$) to its upstream neighbour zones in addition to its own buses, c_i , with the exception of Zone 1, which does not have any upstream neighbour zones. After defining the extended zone bus sets, we recalculated the hermitian matrices of (4.10d and 4.10e) to be able to reformulate the chordal relaxed SDP-VVC problem of (4.19) for the furthest extended zone, as follows:

$$\min_{W_s, P_{DG}, Q_{DG}, T_{n,m}, C_g} f(W) + \sum_{g \in N_g^{\hat{c}_i}} C_g \quad (4.26a)$$

$$p_n^{min} \leq tr(\Phi_{P,n}^\phi W) \leq p_n^{max}, \quad \forall n \in N_g^{\hat{c}_i}, \phi \in \psi_n \quad (4.26b)$$

$$q_n^{min} \leq tr(\Phi_{Q,n}^\phi W) \leq q_n^{max}, \quad \forall n \in N_g^{\hat{c}_i}, \phi \in \psi_n \quad (4.26c)$$

$$v_n^{min} \leq tr(E_n^\phi W) \leq v_n^{max}, \quad \forall n \in N_g^{\hat{c}_i}, \phi \in \psi_n \quad (4.26d)$$

$$tr(\Phi_{P,n}^\phi W) = \sum_{g \in Ng^{\hat{c}_i}} P_{n,g}^\phi - \sum_{d \in Nl^{\hat{c}_i}} P_{n,d}^\phi + \Lambda_n \cdot P_n^\phi \quad (4.26e)$$

$$tr(\Phi_{Q,n}^\phi W) = \sum_{g \in Ng^{\hat{c}_i}} Q_{n,g}^\phi - \sum_{d \in Nl^{\hat{c}_i}} Q_{n,d}^\phi + \sum_{q \in C_s} Q_{n,q}^\phi + \Lambda_n \cdot Q_n^\phi \quad (4.26f)$$

$$T_{n,m}^{min} \leq T_{n,m}^\phi \leq T_{n,m}^{max}, \quad \phi \in \psi_{n,m} \quad (4.26g)$$

$$C_g = c_e^\phi \cdot [(1 + n_{DG}) \cdot P_{DG}], \quad \phi \in \psi_g \quad (4.26h)$$

$$W_s \succeq 0; \quad \forall s \in S \quad (4.26i)$$

$$\begin{bmatrix} (S_{DG}^{max})^2 & P_{DG} & Q_{DG} \\ P_{DG} & 1 & 0 \\ Q_{DG} & 0 & 1 \end{bmatrix} \succeq 0 \quad (4.26j)$$

$$\text{s.t. } (4.5), (4.6), (4.8), (4.9b), (4.15), (4.16). \quad (4.26k)$$

4.4.1.2 Proposed Hierarchical Distributed Solution

Each extended zone is treated as a single standalone distribution network and a related chordal-relaxed SDP-VVC problem (4.26) is formulated. To obtain a solution for the whole distribution system, each extended zone's VVC problem needs to be solved. Therefore, an efficient hierarchical distributed solution (HDS) algorithm is developed to obtain the solution. The detailed process of the HDS for a radial distribution system is explained in the following steps:

1. Select the furthest extended zone in the system as the active extended zone (e.g. Zone \hat{z} in Fig. 4.2), and solve the chordal-relaxed SDP-VVC problem (4.26) for it,
2. Obtain the active and reactive powers of each phase transferred from the upstream neighbour zone to the active extended zone via connection bus as they are given in (4.27a) and (4.27b) for extended zone \hat{z} , respectively.
3. Select the upstream neighbour zone as the next active extended zone (e.g. Zone $z - 1$ in Fig. 4.2),
4. Modify the problem (4.26) by adding the obtained active and reactive powers from (4.27a) and (4.27b) as virtual active/reactive load for the connection bus as formulated in (4.27c) and (4.27d). Also, place an equality constraint on the connection bus voltage (V_k) as given in (4.27e). The voltage equality constraint will force the connection bus voltage to be equal in both zone-related solutions.
5. Solve the modified chordal-relaxed SDP-VVC problem (4.26), and If the active extended zone is equal to Zone 1, then stop this process

6. Otherwise, repeat this process from step 2 until the active extended zone is equal to Zone 1.

$$P_{k,d}^{\phi,\hat{z}} = tr(\Phi_{P,k}^{\phi,\hat{z}} W), \quad \phi \in \psi_k, \quad (4.27a)$$

$$Q_{k,d}^{\phi,\hat{z}} = tr(\Phi_{Q,k}^{\phi,\hat{z}} W), \quad \phi \in \psi_k, \quad (4.27b)$$

$$tr(\Phi_{P,k}^{\phi,(z\hat{-}1)} W) = P_{k,g}^{\phi} - (P_{k,d}^{\phi} + P_{k,d}^{\phi,\hat{z}}), \quad \phi \in \psi_k, \quad (4.27c)$$

$$tr(\Phi_{Q,k}^{\phi,(z\hat{-}1)} W) = Q_{k,g}^{\phi} - (Q_{k,d}^{\phi} + Q_{k,d}^{\phi,\hat{z}}), \quad \phi \in \psi_k, \quad (4.27d)$$

$$tr(E_k^{\phi,(z\hat{-}1)} W) = tr(E_k^{\phi,\hat{z}} W), \quad \phi \in \psi_k. \quad (4.27e)$$

4.4.2 2-Stage Volt/Var Control Algorithm

A 2-stage VVC algorithm is proposed to mitigate the negative effects of renewable energy resources on voltage profile and regulator devices in active distribution systems. These negative effects arise mainly due to fast changes in RESs' output power and from output power forecasting errors.

In the first stage, the VVC problem is solved for day-ahead operation based on forecasted hourly generation and demand profiles. However, in the presence of fast changing RESs' power outputs, voltage profiles may not stay within the permissible limits during inter-hour operations. We thus divide the hour-based time window into 15-minutes time intervals as it is illustrated in Fig. 4.3. We then solve the problem based on 15-minutes load and generation forecasts to ensure the voltage profile stays within the set limits during inter-hour operations. In the second stage, we limit the control action by considering only RESs' controllable active and reactive power outputs; the VR tap positions and shunt capacitors are maintained in the same position determined in the first stage.

In the proposed 2-stage control, VR tap operations are limited, thus prolonging the VR operation life expectancy and decreasing maintenance frequency and operational cost, while ensuring system voltage stays within the limits all times.

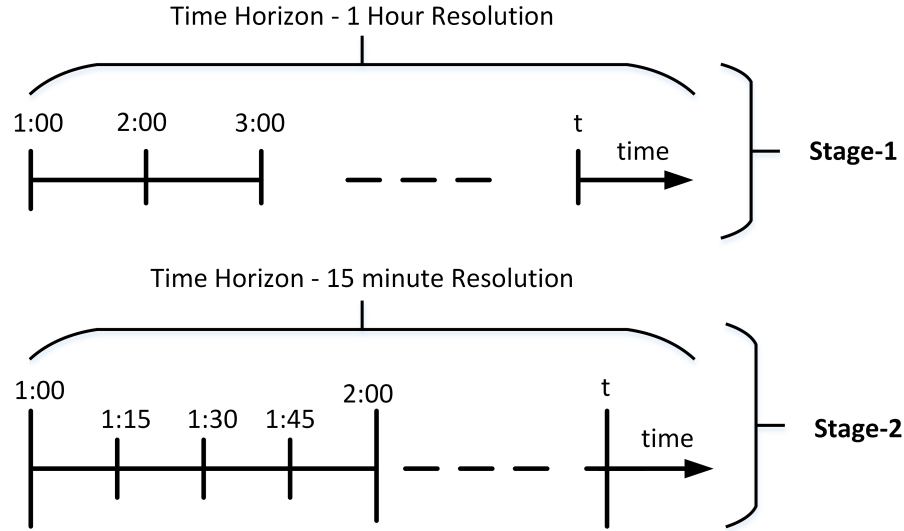


Figure 4.3 Time resolution of the proposed 2-stage control algorithm.

4.5 Case Studies

The proposed chordal relaxed SDP-VVC approach was examined on a modified IEEE-34 bus test system, as shown in Fig. 4.4 [66]. The modified test system has 36 buses in total; 34 of them are original system buses, while 2 buses are virtual (bus 8 and 21 for modelling the two VRs). There are two three-phase VR, and the tap ratios are allowed to operate between 0.95 and 1.05 pu. In discrete tap ratio modelling, $2T_t$ is taken as 4, and the ratio step size ($C_{n,m}$) as 0.0125. A single-phase capacitor bank is connected to bus 13 with reactive power limits of $[-55, 55]$ kVAr. Two three-phase and one single-phase solar-based

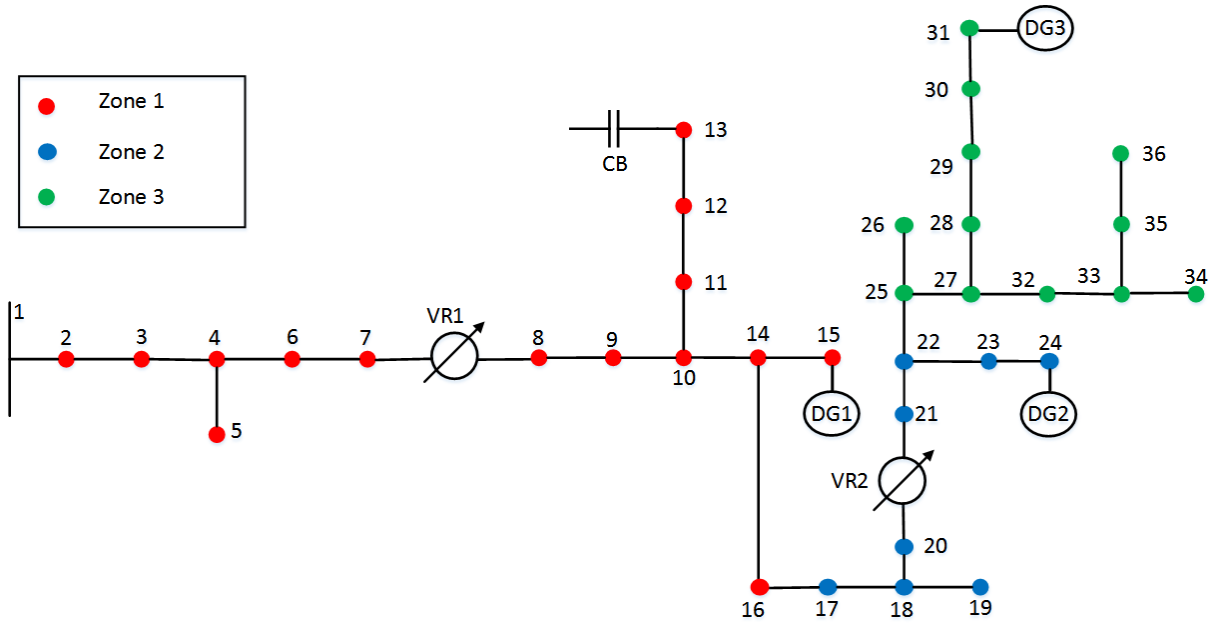


Figure 4.4 One-line diagram of the modified IEEE-34 bus test system.

RESs are connected to bus 15, 24, and 31 via an inverter of the power loss factor of 0.02. All DGs are assumed to operate at a power factor of $0 \leq PF_{DG} \leq 1$. Detailed data for the connected DGs is presented in Table 4.2. The electricity cost for the substation bus is assumed to be 10 ¢/kWh.

Table 4.2 Renewable DG Data

Phase	c_e (¢/kWh)	P_g^{max} (kW)	P_g^{min} (kW)	S_g^{max} (kVA)
a	9.1	250	0	400
b	9.2	250	0	350
c	9.3	250	0	350

Typical hourly load profiles for a commercial consumer, an office building, (adopted from [74]), and for industrial and residential customers (adopted from [75]) are given in

Fig. 4.5.

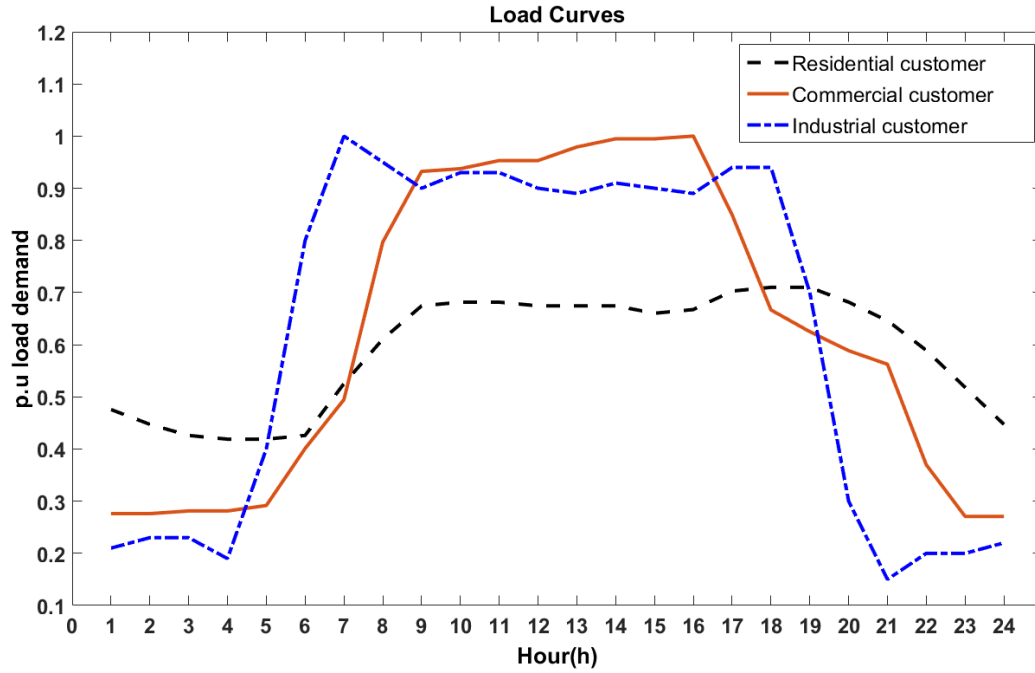


Figure 4.5 Daily load profiles for different customer types.

For the 2-stage control algorithm, 15-minute interval load profiles are obtained from hourly load forecast via simple linear interpolation. For the solar-based renewable DG power output, the forecasted and actual solar power values are obtained from a transmission company in Germany for the day of 01/01/2015 [76], and the data is scaled down to be able to use it at a distribution level. In order to obtain hourly solar power forecast from the available 15-minute solar data, we take the average of four 15-minute interval forecasts in an hour.

All the simulations were performed on a personal computer with an Intel Core 2 Duo 2.4 GHz processor and 8 GB RAM. We performed the discrete SVR tap ratio modelling simulations in MATLAB using YALMIP toolbox [77] and its branch-and-bound (BAB)

solver, while the continuous SVR tap ratio simulations were performed by using MOSEK optimization software [78].

4.5.1 Base Case (Single Zone, Centralized Solution) Simulation

In the base case simulation, the system is threaded as a single control zone, and the problem is solved in a centralized approach for day-ahead hourly operation using forecasted generation and load profiles. The objective function is power loss minimization, and both continuous and discrete voltage regulator tap ratio modelling have been considered. The daily simulation results of active power losses, generation cost, solution time, number of tap movements, and voltage deviation values are reported in Table 4.3.

Table 4.3 Centralized and Distributed Solution Results

Objective Function	Continuous Tap Modelling		Discrete Tap Modelling	
	Centralized	Distributed	Centralized	Distributed
Daily Generation Cost (CAD)	2,009.80	2,011.80	2,017.60	2,012.50
Daily Power Losses (pu)	0.1238	0.1250	0.1248	0.1251
Daily Tap Position Movement	6	2	85	65
Solution Time (sec)	63	75	316	135
Total Voltage Deviation (Eq. 4.23) (pu)	0.1001	0.0515	0.5346	0.4463

Continuous tap ratio modelling has achieved lower generation costs and power loss compared to discrete tap modelling due to that there is no limitation on what the tap ratio could be as long as it stays in the tap ratio limits. Lower voltage deviation is also obtained in the continuous case because of the limitless tap ratio value possibility compared to a discrete tap ratio that has limited tap ratio options. Continuous tap ratio modelling also yielded a lower number of tap movements, along with achieving a lower solution time.

The daily power outputs of a substation and renewable energy resources are reported in Table 4.4. For continuous tap modelling, active power demand is supplied by a substation and DG1, while in discrete tap modelling the active power outputs of DGs have dropped significantly. The reason behind having no active power supply from the DGs in discrete case is the high electricity price for DG output. We observed that if the price for the RESs is decreased, then the RESs' output power increased. For the reactive power, there is not much change in injection for both tap ratio modelling cases.

Table 4.4 Base Case Centralized Solution Daily Power Outputs of Generators

Power Supply	Continuous Tap		Discrete Tap	
	Active (kW)	Reactive ($kVAr$)	Active (kW)	Reactive ($kVAr$)
Substation Bus	19,530	620	20,170	960
DG1	540	830	0	890
DG2	29	5,770	0	5,430
DG3	31	5,200	0	5,170

4.5.2 Scenario 1 (3-Zones, Distributed Solution) Simulation

In scenario 1, the system is divided into three zones based on the customer types, namely Zone-1 (all loads are residential), Zone-2 (all loads are commercial), and Zone-3 (all loads are industrial) as shown in Fig. 4.4. The system has been solved using the proposed hierarchical distributed solution algorithm with the objective of power loss minimization for day-ahead operation using forecasted 1-hour interval load and generation profiles. Daily power losses, total power generation cost, solution time, and number of VR tap movements are obtained for a day-ahead hourly operation for both continuous and discrete tap ratio modelling cases. The results are shown in Table 4.3. For continuous tap modelling, the

proposed distributed solution achieves less tap movements (66% decrease) and voltage deviation (48% decrease); however, it slightly increases the daily power generation cost (0.1% increase) and solution time (20% increase). The rise in solution time is due to the YALMIP startup process that has to be repeated for each zone, in other words YALMIP needs to repeat the internal startup process 3 times to obtain the solution for 3 zones in a distributed solution algorithm compared to 1 internal startup process in the centralized approach.

On the other hand, for discrete tap ratio modelling, the proposed distributed solution outperforms the centralized algorithm in daily power generation cost (0.25% decrease), tap movements (23% decrease), solution time (57% decrease) and voltage deviation (16.5% decrease). In particular, it decreases the total daily tap movement by 23% without causing any power generation cost increase. It also decreases the total solution time by 57% compared to the centralized approach in discrete tap ratio.

4.5.3 Scenario 2 Simulation

In scenario 2, we solved the problem with a hierarchical distributed solution algorithm and adjusted the objectives according to each zone's own characteristics and requirements. For the residential area, the control objective is to minimize the active power loss, while in the industrial and commercial zones, the objective function aims at power loss minimization and flat voltage profiles.

The scenario 2 simulation results are shown in Table 4.5, and continuous tap modelling yields less tap movements and voltage deviation compared to discrete tap ratio modelling. Achieving less voltage deviation in the continuous tap ratio case is due to the unlimited tap ratio options between the tap limits, while it is limited in the discrete tap ratio modelling

Table 4.5 Scenario-2 Hierarchical Distributed Daily Simulation Results

Objective Function	Continuous Tap	Discrete Tap
Daily Generation Cost (CAD)	2,012.10	2,013.30
Daily Power Losses (pu)	0.1250	0.1251
Daily Tap Position Movement	0	12
Solution Time (sec)	82	140
Total Voltage Deviation (Eq. 4.23) (pu)	0.0197	0.1748
Zone 1 Total Voltage Deviation (pu)	0.01972	0.17482
Zone 2 Total Voltage Deviation (pu)	0	0
Zone 3 Total Voltage Deviation (pu)	0	0

that can take only certain number of tap ratios which may deviate the ratio from the best possible value. In terms of daily power generation cost and power loss, both tap ratio modelling cases yield very similar results.

4.5.4 Scenario 3 Simulation

The novel contribution of this scenario is to introduce tap movement minimization in a convex VVC problem. This scenario is only applicable to discrete tap ratio modelling. The total objective function is to minimize the power loss and tap movement summation, $f(W) = f_0(W) + f_2(W)$. The simulation results are given in Table 4.6. As it can be seen from the Table 4.6, the daily number of tap movements has been decreased by 38% in addition to achieving less voltage deviation (27% decrease); while the daily total power generation cost and total power loss is increased only by %0.23 and by %0.4, respectively. VR-1 and VR-2 daily tap positions are given in Fig. 4.6 and Fig. 4.7, respectively, for the cases of no tap limit and with tap limit constraints.

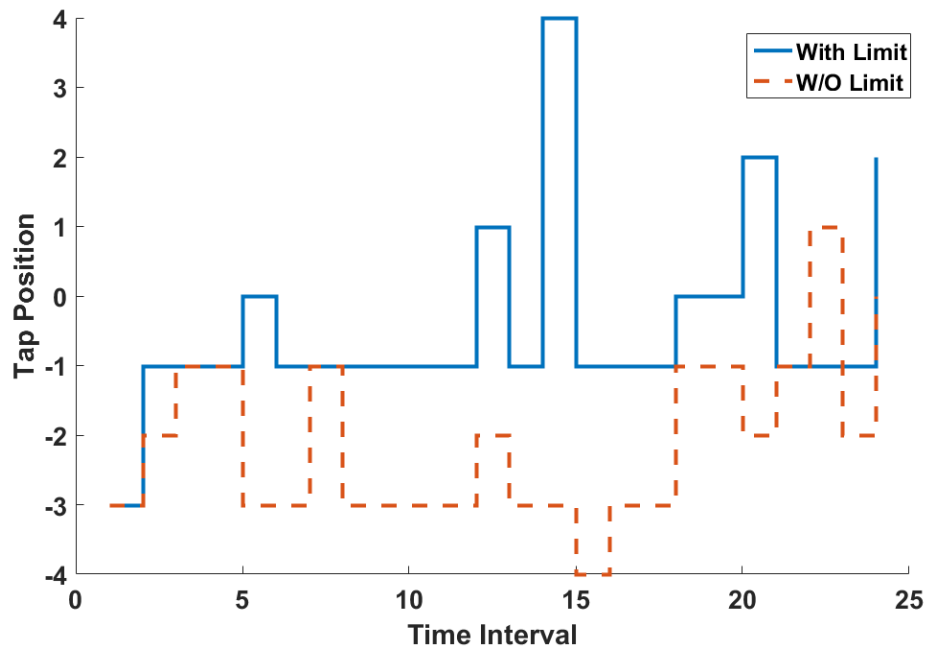


Figure 4.6 Daily VR-1 tap positions in Scenario 3.

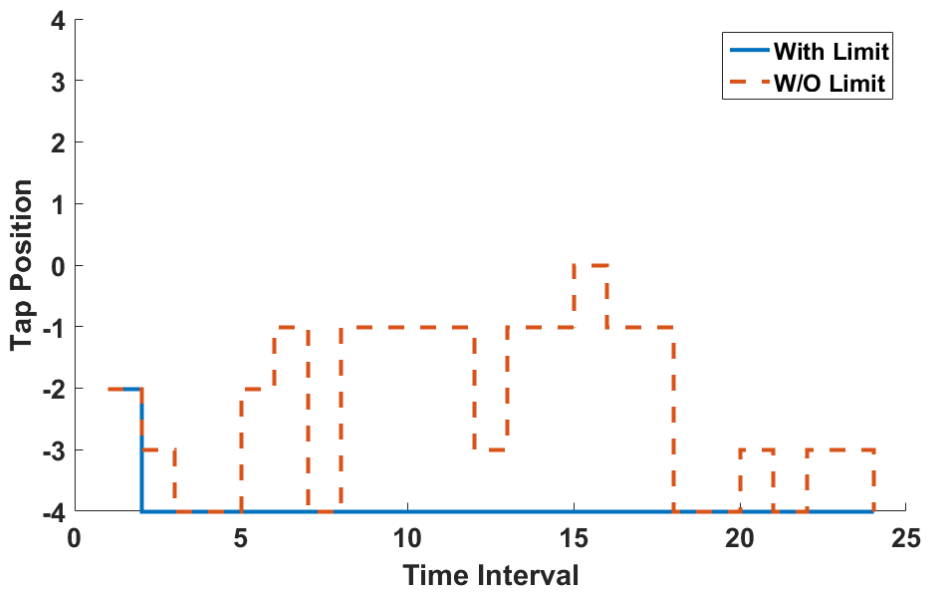


Figure 4.7 Daily VR-2 tap positions in Scenario 3.

Table 4.6 Scenario-3 Hierarchical Distributed Daily Simulation Results ($w_2 = 200$)

Objective Function	W/O Tap Limits	With Tap Limits
Daily Generation Cost (CAD)	2,006.90	2,011.20
Daily Power Losses (pu)	0.1240	0.1245
Daily Tap Position Movement	47	29
Solution Time (sec)	135	160
Total Voltage Deviation (Eq. 4.23) (pu)	0.4716	0.3444

4.5.5 Scenario 4 Simulation

In this scenario, we investigate the system under a two-stage solution algorithm with discrete tap ratio modelling. The main objective is to mitigate the impact of renewable energy resources' power volatility on the VR tap movements and the system voltage profile. Since 1-hour control intervals are too long to mitigate fast changing RESs output power, the VVC problem is considered for each 15-minute interval for two different cases: 1.) VR control devices are used to regulate the voltage along with other control entities, and 2.) only RESs' active and reactive power adjustment capability (absorb and/or inject) is used to regulate system voltage. In the second case, the VR tap positions are kept fixed during inter-hour intervals (e.g. hh:00, hh:15, hh:30, hh:45, hh+1:00) at the position that was obtained from the 1-hour interval solution that is performed at the beginning of the operation cycle. The comparison of the daily tap movement number for both single- and two-stage control is presented in Table 4.7. For the single-stage day-ahead operation control, we used 15-minute intervals of actual solar DG's active power output values, which is obtained for the date of 01/01/2015 and given in Fig.4.8 [76]. For the two-stage control

Table 4.7 Scenario-4 Centralized Daily Simulation Results for Tap Movement

Tap Variable Type	Single-Stage control	Two-Stage Control
Discrete Tap	36	14

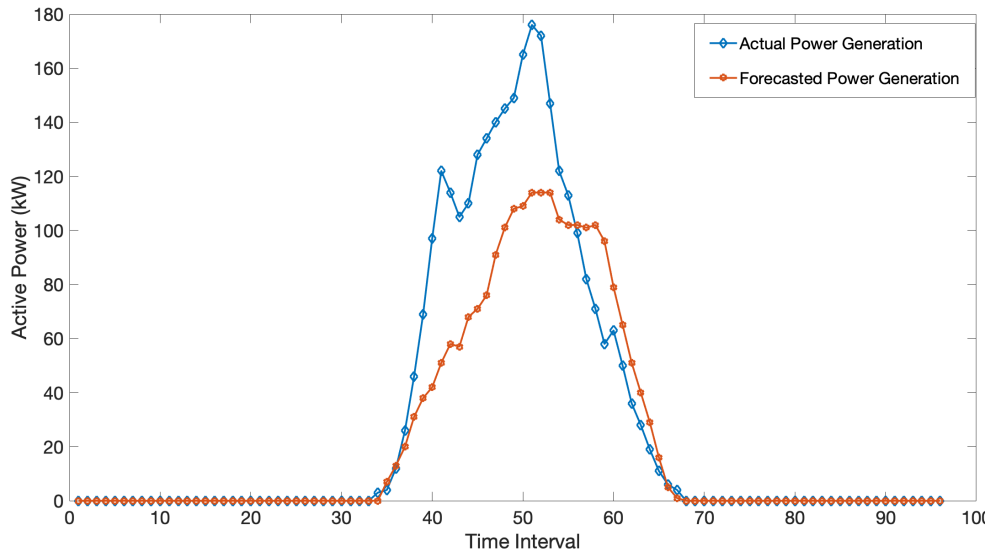


Figure 4.8 Actual and forecasted solar DG’s active power output for 15-minutes intervals.

case, in the first layer, VR tap positions are obtained from the centralized solution based on forecasted hourly solar DG’s active power outputs, which is given in Fig. 4.9. In the second layer, the problem is solved based on 15-minutes actual active power values while keeping the tap position fixed during inter-hour time steps as they are obtained from the first layer solution. As it can be seen from Table 4.7, the two-stage control algorithm achieved a 61% decrease in daily tap movement in discrete tap ratio modelling. The daily tap profile of each VR is given for both single and two-stage solution algorithms with discrete tap ratio modelling in Fig. 4.10 and Fig. 4.11, respectively.

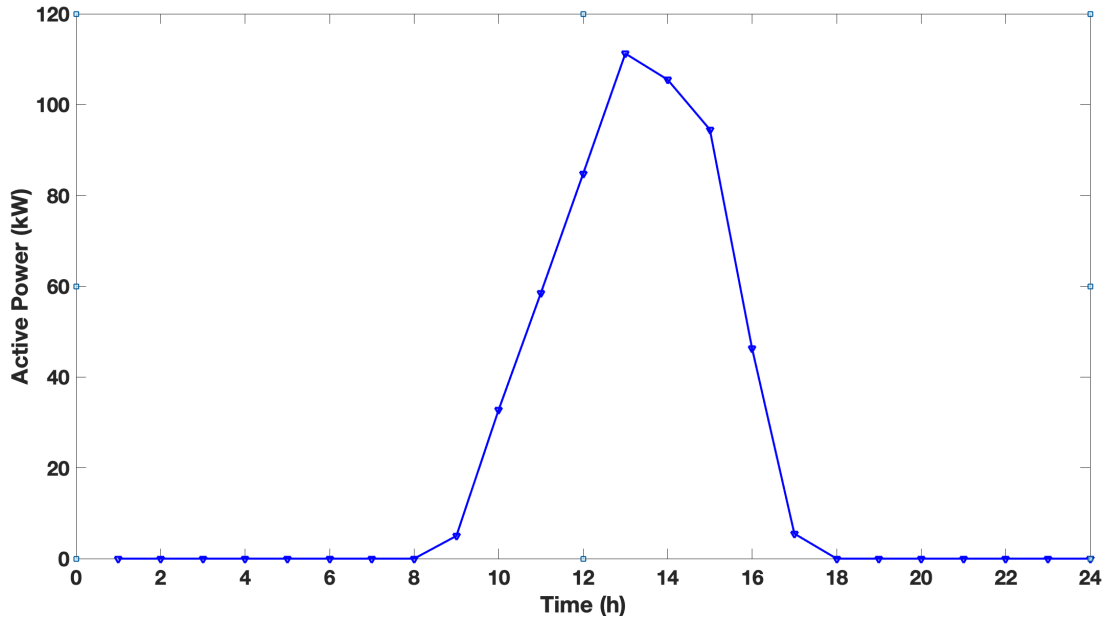


Figure 4.9 Hourly forecasted solar-based RES active power output.

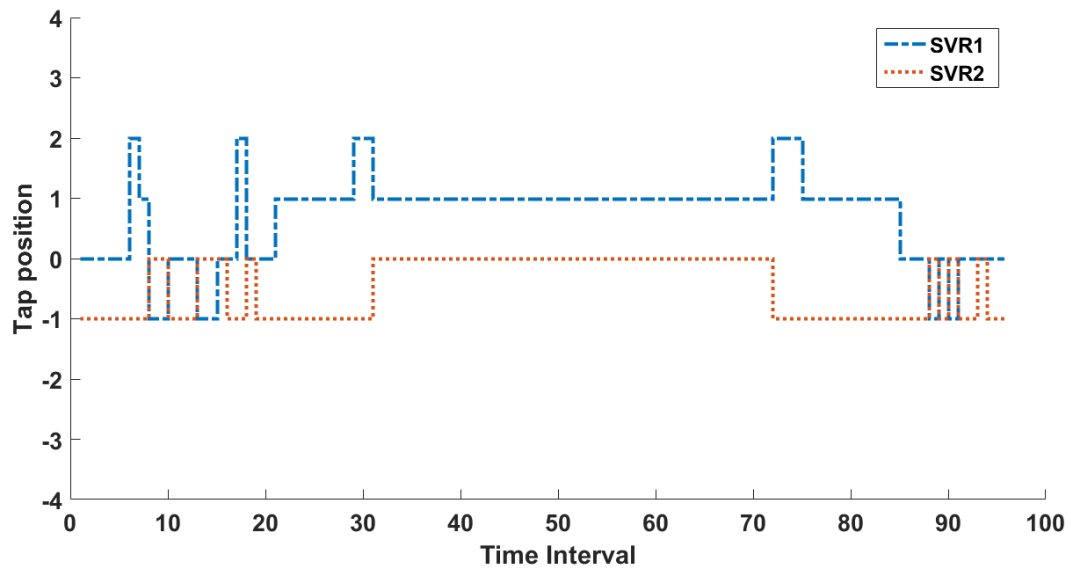


Figure 4.10 VR tap positions for single-stage control solution with discrete tap modelling.

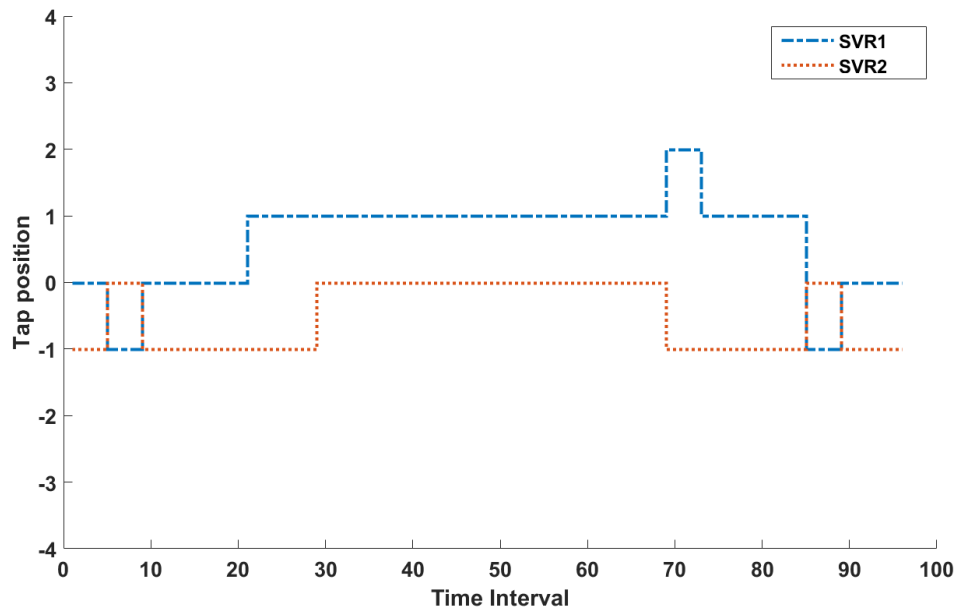


Figure 4.11 VR tap positions for two-stage control solution with discrete tap modelling.

Injected reactive power from each DG is provided for single and two-stage solution algorithms in Fig. 4.12 and Fig. 4.13, respectively. DG2 and DG3 provide a large amount of reactive power to the system due to being three-phase DG.

4.5.6 Simulations Discussion

In scenario 1, neither the centralized nor the distributed approach has dominated in achieving better results. Each method has its own strengths and weaknesses; therefore, it is up to the system operator's preferences to prefer one over the other. For scenario 2, continuous tap modelling outperforms the discrete tap modelling in every objective category. However, it is worth noting that the continuous tap ratios have to be rounded to the nearest integer number, which may create voltage violations in some cases. Tap movement minimization

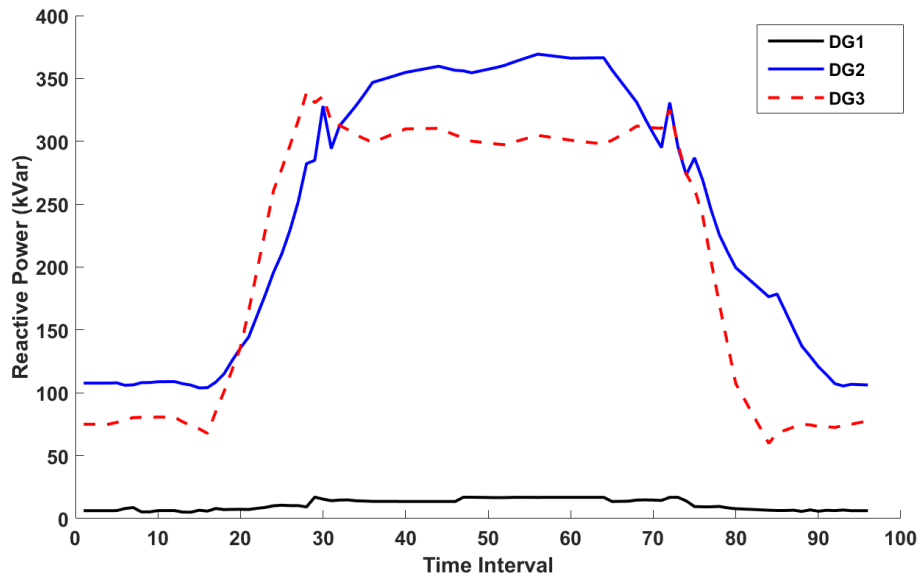


Figure 4.12 Reactive power injection of each DG for single-stage control with discrete tap modelling.

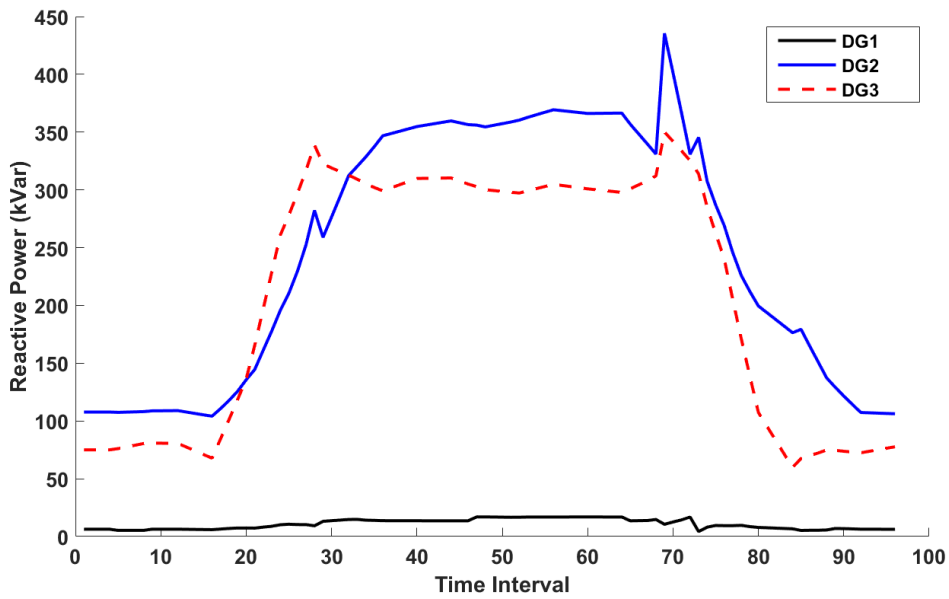


Figure 4.13 Reactive power injection of each DG for two-stage control with discrete tap modelling.

utilization in scenario 3 reduced the total tap movement effectively, which will prolong the life of voltage regulators. In scenario 4, by using two-stage control the negative impact of renewable RESs has been decreased, which may allow more distributed RES penetration into the system.

4.6 Conclusion

In emerging distribution systems, centralized control algorithms are not favourable due to their high computational and communication burdens. In order to ease these burdens, a novel hierarchical distributed SDP-VVC algorithm has been developed for active distribution networks, while considering continuous and discrete tap ratio modellings. The proposed distributed algorithm significantly decreases the solution time, in comparison to centralized control in discrete tap modelling. Furthermore, a practical classification technique based on consumer type has been proposed in order to cluster the network into sub-systems based on electricity consumer types, wherein each zone is treated according to its unique requirements and characteristics. In addition, to achieve an overall minimal cost, a two-stage control algorithm has been developed that aims for tap movement minimization in a convex VVC formulation. The first-stage control is based on hourly forecasted generation and loads, while in the second-stage 15-minute interval forecasted values have been used in the second stage. Both hourly and inter-hourly techniques decrease the total daily tap movement, with minimal change in voltage deviation and without any significant increase in generation costs. All the obtained results are globally optimal due to having a rank-1 solution matrix.

Chapter 5

Synopsis and Future Research

5.1 Synopsis

The main goal of this dissertation was to develop novel VVC algorithms in an attempt to tackle the current challenges associated with Volt/Var control in active distribution systems. The main objective of the first part of the study was to develop a generic VVC algorithm for different system operating conditions. To achieve this objective, a novel state-based VVC algorithm was developed in Chapter 3 for three different grid operating states. The operating states were identified by using a system state index that was calculated based on measured system voltage values from critical buses. The problem was then formulated as a non-linear optimization problem with various objectives for different operating states. A heuristic-based genetic algorithm optimization technique was used to solve the problem. For the emergency operating state, a novel rule-based VVC algorithm was implemented to be able to take quick actions in order to regulate the voltage. The simulation results demonstrated that the proposed VVC algorithm operates the system at

its optimum condition, while also improving the voltage profile.

An economic feasibility analysis was also conducted, in terms of total cost of each control strategy. During the normal operation state, it was found that the DG participation is not a cost-effective option. The results also demonstrated that involving DGs in VVC control was not always an optimum solution in state B, which may cause monetary losses for the DG owners. It was also observed that the proposed rule-based algorithm for the emergency state was very efficient to bring the system back into normal operation conditions in a very short amount of time. The main challenge of the solution algorithm used in this developed control strategy was that it does not guarantee the optimal solution and requires a long computational time, especially for larger power systems with thousands of buses.

In the second part of the thesis, the main objective was to develop a zone-based VVC algorithm in an attempt to meet different customers' requirements, while also obtaining an optimal solution with a short computational time. To achieve this objective, the system was divided into multiple zones based on different customer types in Chapter 5, in an attempt to satisfy their needs by considering different zone-oriented objective functions. Next, the VVC problem was formulated as a distributed convex optimization, which was to primarily tackle the long solution time of heuristic-based solution algorithms, along with guaranteeing the optimal solution of the problem. As such, in order to solve the convex optimization problem, a novel hierarchical distributed convex solution algorithm that requires no iterative process and penalty parameter was developed. In addition to this, a 2-stage VVC control methodology that minimizes the impact of RESs on voltage profiles and voltage regulators was developed.

In summary, the contributions of the thesis can be stated as follows:

- The development of a comprehensive, state-based VVC control for active distribution

systems under high penetration of distributed RESs.

- The achievement of optimal system operation under VVC by adjusting the objectives and control devices according to different system operating conditions.
- The development of operational flexibility for distribution system operators for multiple possible operating conditions.
- The development of a rule-based VVC algorithm for the emergency operating state, where applying optimization algorithms is infeasible due to the need for quick control actions.
- The development of a practical classification technique to cluster the network into sub-systems based on consumer type, wherein each zone is treated according to its unique requirements and characteristics.
- The development of a comprehensive, zone-oriented distributed convex VVC control algorithm for active distribution systems.
- The development of a novel hierarchical distributed control algorithm that requires no iterative process and no penalty parameter.
- The development of a 2-stage control algorithm to minimize the tap operations of voltage regulators in the presence of renewable distributed generations.

5.2 Future Work Directions

While this study presents a new Volt/Var control methodology in order to address the current power system requirements and challenges in the presence of high RESs penetration,

there remains the possibility of future research ideas based on what has been presented:

- The application of the developed hierarchical distributed solution to different problems in power systems.
- The application of the proposed zone-oriented convex VVC algorithm to larger systems.
- The implementation and investigation of the proposed VVC algorithms under high-level penetration of electric vehicles.

Appendix A

Sub-matrix W_s Construction

A 3-bus system will be used to illustrate the creation of sub-matrix W_s from square matrix W . The voltage vector V can be written as follows:

$$V = \begin{bmatrix} V_0^T & V_1^T & V_2^T \end{bmatrix}^T,$$

where $V_i = \begin{bmatrix} V_i^a & V_i^b & V_i^c \end{bmatrix}$ for $i = 0, 1, 2$. Square matrix W can be defined as below using voltage vector V :

$$W = VV^H = \begin{bmatrix} V_0 \\ V_1 \\ V_2 \end{bmatrix} \begin{bmatrix} V_0 \\ V_1 \\ V_2 \end{bmatrix}^H.$$

By defining a new variable $W_{n,m}^{\phi,\psi}$ to substitute the nonlinear terms of $V_n^\phi \cdot V_m^\psi$, then a 9×9 square matrix W can be obtained as follows:

$$W = \begin{bmatrix} W_{0,0} & W_{0,1} & 0 \\ W_{1,0} & W_{1,1} & W_{1,2} \\ 0 & W_{2,1} & W_{2,2} \end{bmatrix},$$

Sub-matrices that correspond to each maximal clique in the chordal graph can be defined as follows:

$$\begin{bmatrix} V_0 \\ V_1 \end{bmatrix} \cdot \begin{bmatrix} V_0 \\ V_1 \end{bmatrix}^H \Rightarrow W_1 = \begin{bmatrix} W_{0,0} & W_{0,1} \\ W_{1,0} & W_{1,1} \end{bmatrix};$$

$$\begin{bmatrix} V_1 \\ V_2 \end{bmatrix} \cdot \begin{bmatrix} V_1 \\ V_2 \end{bmatrix}^H \Rightarrow W_2 = \begin{bmatrix} W_{1,1} & W_{1,2} \\ W_{2,1} & W_{2,2} \end{bmatrix}.$$

Both W_1 and W_2 are 6×6 square matrices which represent 3-phase lines of a 3-bus system.

References

- [1] *American National Standard for Electric Power Systems and Equipment Voltage Ratings (60 Hertz)*, ANSI C84.1 Std., 2011.
- [2] *Renewable capacity statistics 2019*. Abu Dhabi: International Renewable Energy Agency, 2019.
- [3] P. Wang, D. Liang, J. Yi, P. Lyons, P. Davison, and P. Taylor, “Integrating electrical energy storage into coordinated voltage control schemes for distribution networks,” *Smart Grid, IEEE Transactions on*, vol. 5, no. 2, pp. 1018–1032, March 2014.
- [4] J. von Appen, T. Stetz, M. Braun, and A. Schmiegel, “Local voltage control strategies for pv storage systems in distribution grids,” *Smart Grid, IEEE Transactions on*, vol. 5, no. 2, pp. 1002–1009, March 2014.
- [5] M. Nick, M. Hohmann, R. Cherkaoui, and M. Paolone, “On the optimal placement of distributed storage systems for voltage control in active distribution networks,” in *Innovative Smart Grid Technologies (ISGT Europe), 2012 3rd IEEE PES International Conference and Exhibition on*, Oct 2012, pp. 1–6.

- [6] G. Sulligoi and M. Chiandone, "Voltage rise mitigation in distribution networks using generators automatic reactive power controls," in *Power and Energy Society General Meeting, 2012 IEEE*, July 2012, pp. 1–5.
- [7] E. A. Paaso, Y. Liao, and A. M. Cramer, "Formulation and solution of distribution system voltage and {VAR} control with distributed generation as a mixed integer non-linear programming problem," *Electric Power Systems Research*, vol. 108, no. 0, pp. 164 – 169, 2014.
- [8] M. Elkhatib, R. Shatshat, and M. Salama, "Decentralized reactive power control for advanced distribution automation systems," *Smart Grid, IEEE Transactions on*, vol. 3, no. 3, pp. 1482–1490, Sept 2012.
- [9] J. Barr and R. Majumder, "Integration of distributed generation in the volt/var management system for active distribution networks," *Smart Grid, IEEE Transactions on*, vol. 6, no. 2, pp. 576–586, March 2015.
- [10] M. Vaziri, S. Vadhva, T. Oneal, and M. Johnson, "Smart grid, distributed generation, and standards," in *Power and Energy Society General Meeting, 2011 IEEE*, July 2011, pp. 1–8.
- [11] S. Civanlar and J. Grainger, "Volt/var control on distribution systems with lateral branches using shunt capacitors and voltage regulators part ii: The solution method," *Power Apparatus and Systems, IEEE Transactions on*, vol. PAS-104, no. 11, pp. 3284–3290, Nov 1985.
- [12] M. Kaplan, "Optimization of number, location, size, control type, and control setting of shunt capacitors on radial distribution feeders," *Power Engineering Review, IEEE*, vol. PER-4, no. 9, pp. 59–59, Sept 1984.

- [13] H. Dura, “Optimum number, location, and size of shunt capacitors in radial distribution feeders a dynamic programming approach,” *Power Apparatus and Systems, IEEE Transactions on*, vol. PAS-87, no. 9, pp. 1769–1774, Sept 1968.
- [14] H.-D. Chiang, J.-C. Wang, O. Cockings, and H.-D. Shin, “Optimal capacitor placements in distribution systems. i. a new formulation and the overall problem,” *Power Delivery, IEEE Transactions on*, vol. 5, no. 2, pp. 634–642, Apr 1990.
- [15] D. Sattianadan, M. Sudhakaran, K. Vijayakumar, and S. Vidyasagar, “Optimal placement of capacitor in radial distribution system using pso,” in *Sustainable Energy and Intelligent Systems (SEISCON 2011), International Conference on*, July 2011, pp. 326–331.
- [16] Z. Hu, X. Wang, H. Chen, and G. Taylor, “Volt/var control in distribution systems using a time-interval based approach,” *Generation, Transmission and Distribution, IEE Proceedings-*, vol. 150, no. 5, pp. 548–554, Sept 2003.
- [17] F. Tomasevic, K. Baranasic, and M. Delimar, “Reactive power optimization based on load profile partitioning,” in *Energy Conference (ENERGYCON), 2014 IEEE International*, May 2014, pp. 627–632.
- [18] S. Auchariyamet and S. Sirisumrannukul, “Volt/var control in distribution systems by fuzzy multiobjective and particle swarm,” in *Electrical Engineering/Electronics, Computer, Telecommunications and Information Technology, 2009. ECTI-CON 2009. 6th International Conference on*, vol. 01, May 2009, pp. 234–237.
- [19] P. Bauer and S. de Haan, “New concept for voltage control,” in *Power Electronic Drives and Energy Systems for Industrial Growth, 1998. Proceedings. 1998 International Conference on*, vol. 2, Dec 1998, pp. 918–923 Vol. 2.

- [20] F.-C. Lu and Y.-Y. Hsu, "Reactive power/voltage control in a distribution substation using dynamic programming," *Generation, Transmission and Distribution, IEE Proceedings-*, vol. 142, no. 6, pp. 639–645, Nov 1995.
- [21] M. Baran and M.-Y. Hsu, "Volt/var control at distribution substations," *Power Systems, IEEE Transactions on*, vol. 14, no. 1, pp. 312–318, Feb 1999.
- [22] T. Niknam, A. Ranjbar, and A. Shirani, "Impact of distributed generation on volt/var control in distribution networks," in *Power Tech Conference Proceedings, 2003 IEEE Bologna*, vol. 3, June 2003, pp. 1–7.
- [23] H. Yujun and M. Petit, "Active voltage control using distributed generation on distribution networks," in *PowerTech (POWERTECH), 2013 IEEE Grenoble*, June 2013, pp. 1–6.
- [24] D. Ranamuka, A. Agalgaonkar, and K. Muttaqi, "Online voltage control in distribution systems with multiple voltage regulating devices," *Sustainable Energy, IEEE Transactions on*, vol. 5, no. 2, pp. 617–628, April 2014.
- [25] Z. Ziadi, M. Oshiro, T. Senjyu, A. Yona, N. Urasaki, T. Funabashi, and C.-H. Kim, "Optimal voltage control using inverters interfaced with pv systems considering forecast error in a distribution system," *Sustainable Energy, IEEE Transactions on*, vol. 5, no. 2, pp. 682–690, April 2014.
- [26] J. Jung, A. Onen, R. Arghandeh, and R. P. Broadwater, "Coordinated control of automated devices and photovoltaic generators for voltage rise mitigation in power distribution circuits," *Renewable Energy*, vol. 66, no. 0, pp. 532 – 540, 2014.

- [27] A. Kulmala, S. Repo, and P. Jarventausta, “Coordinated voltage control in distribution networks including several distributed energy resources,” *Smart Grid, IEEE Transactions on*, vol. 5, no. 4, pp. 2010–2020, July 2014.
- [28] T. Sansawatt, L. Ochoa, and G. Harrison, “Integrating distributed generation using decentralised voltage regulation,” in *Power and Energy Society General Meeting, 2010 IEEE*, July 2010, pp. 1–6.
- [29] V. Calderaro, V. Galdi, G. Massa, and A. Piccolo, “Distributed generation and local voltage regulation: An approach based on sensitivity analysis,” in *Innovative Smart Grid Technologies (ISGT Europe), 2011 2nd IEEE PES International Conference and Exhibition on*, Dec 2011, pp. 1–8.
- [30] V. Calderaro, G. Conio, V. Galdi, G. Massa, and A. Piccolo, “Optimal decentralized voltage control for distribution systems with inverter-based distributed generators,” *Power Systems, IEEE Transactions on*, vol. 29, no. 1, pp. 230–241, Jan 2014.
- [31] F. Viawan and D. Karlsson, “Combined local and remote voltage and reactive power control in the presence of induction machine distributed generation,” *Power Systems, IEEE Transactions on*, vol. 22, no. 4, pp. 2003–2012, Nov 2007.
- [32] V. Calderaro, G. Conio, V. Galdi, G. Massa, and A. Piccolo, “Active management of renewable energy sources for maximizing power production,” *International Journal of Electrical Power & Energy Systems*, vol. 57, no. 0, pp. 64 – 72, 2014.
- [33] J. Petintin and M. Shaaban, “Voltage regulation in a smart distribution system incorporating variable renewable generation,” in *Innovative Smart Grid Technologies - Asia (ISGT Asia), 2014 IEEE*, May 2014, pp. 583–588.

- [34] H. Ma and D. Hill, “Adaptive coordinated voltage control;part i: Basic scheme,” *Power Systems, IEEE Transactions on*, vol. 29, no. 4, pp. 1546–1553, July 2014.
- [35] M. El Moursi, H. Zeineldin, J. Kirtley, and K. Alobeidli, “A dynamic master/slave reactive power-management scheme for smart grids with distributed generation,” *Power Delivery, IEEE Transactions on*, vol. 29, no. 3, pp. 1157–1167, June 2014.
- [36] G. Valverde and T. Van Cutsem, “Model predictive control of voltages in active distribution networks,” *Smart Grid, IEEE Transactions on*, vol. 4, no. 4, pp. 2152–2161, Dec 2013.
- [37] Y.-J. Kim, S.-J. Ahn, P.-I. Hwang, G.-C. Pyo, and S.-I. Moon, “Coordinated control of a dg and voltage control devices using a dynamic programming algorithm,” *Power Systems, IEEE Transactions on*, vol. 28, no. 1, pp. 42–51, Feb 2013.
- [38] M. Krok and S. Gene, “A coordinated optimization approach to volt/var control for large power distribution networks,” in *American Control Conference (ACC), 2011*, June 2011, pp. 1145–1150.
- [39] Y. Agalgaonkar, B. Pal, and R. Jabr, “Distribution voltage control considering the impact of pv generation on tap changers and autonomous regulators,” *Power Systems, IEEE Transactions on*, vol. 29, no. 1, pp. 182–192, Jan 2014.
- [40] X. Liu, A. Aichhorn, L. Liu, and H. Li, “Coordinated control of distributed energy storage system with tap changer transformers for voltage rise mitigation under high photovoltaic penetration,” *Smart Grid, IEEE Transactions on*, vol. 3, no. 2, pp. 897–906, June 2012.
- [41] M. Kabir, Y. Mishra, G. Ledwich, Z. Dong, and K. Wong, “Coordinated control of grid-connected photovoltaic reactive power and battery energy storage systems to

- improve the voltage profile of a residential distribution feeder,” *Industrial Informatics, IEEE Transactions on*, vol. 10, no. 2, pp. 967–977, May 2014.
- [42] Y. Yang, H. Li, A. Aichhorn, J. Zheng, and M. Greenleaf, “Sizing strategy of distributed battery storage system with high penetration of photovoltaic for voltage regulation and peak load shaving,” *Smart Grid, IEEE Transactions on*, vol. 5, no. 2, pp. 982–991, March 2014.
- [43] Z. Ziadi, M. Oshiro, T. Senjyu, A. Yona, N. Urasaki, T. Funabashi, and C.-H. Kim, “Optimal voltage control using inverters interfaced with pv systems considering forecast error in a distribution system,” *Sustainable Energy, IEEE Transactions on*, vol. 5, no. 2, pp. 682–690, April 2014.
- [44] K. Muttaqi, A. Le, M. Negnevitsky, and G. Ledwich, “A coordinated voltage control approach for coordination of oltc, voltage regulator and dg to regulate voltage in a distribution feeder,” in *Industry Applications Society Annual Meeting, 2013 IEEE*, Oct 2013, pp. 1–8.
- [45] N. Daratha, B. Das, and J. Sharma, “Coordination between oltc and svc for voltage regulation in unbalanced distribution system distributed generation,” *Power Systems, IEEE Transactions on*, vol. 29, no. 1, pp. 289–299, Jan 2014.
- [46] A. Zakariazadeh, O. Homaei, S. Jadid, and P. Siano, “A new approach for real time voltage control using demand response in an automated distribution system,” *Applied Energy*, vol. 117, no. 0, pp. 157 – 166, 2014.
- [47] U. Eminoglu and M. H. Hocaoglu, “A network topology-based voltage stability index for radial distribution networks,” *International Journal of Power & Energy Systems*, vol. 29, no. 2, pp. 131–143, 2009.

- [48] A. Keane, L. Ochoa, E. Vittal, C. Dent, and G. Harrison, “Enhanced utilization of voltage control resources with distributed generation,” *Power Systems, IEEE Transactions on*, vol. 26, no. 1, pp. 252–260, Feb 2011.
- [49] D. Dohnal, “On-load tap-changers for power transfers,” Maschinenfabrik Reinhausen GmbH, Tech. Rep. F0126405, Tech. Rep., 2013.
- [50] P. Li, H. Ji, C. Wang, J. Zhao, G. Song, F. Ding, and J. Wu, “Coordinated control method of voltage and reactive power for active distribution networks based on soft open point,” *IEEE Transactions on Sustainable Energy*, vol. 8, no. 4, pp. 1430–1442, Oct 2017.
- [51] A. Nayan, “Reactive power planning using pso with modified dynamic inertia parameter,” in *Power and Energy Systems Conference: Towards Sustainable Energy, 2014*, March 2014, pp. 1–6.
- [52] O. P. Authority. (2014) Fit price schedule. [Online]. Available: <http://fit.powerauthority.on.ca/program-resources/price-schedule>
- [53] N. Srinivas and K. Deb, “Multiobjective optimization using nondominated sorting in genetic algorithms,” *Evolutionary Computation*, vol. 2, no. 3, pp. 221–248, Sept 1994.
- [54] K. Deb, A. Pratap, S. Agarwal, and T. Meyarivan, “A fast and elitist multiobjective genetic algorithm: Nsga-ii,” *IEEE Transactions on Evolutionary Computation*, vol. 6, no. 2, pp. 182–197, Apr 2002.
- [55] C. J. Ye and M. X. Huang, “Multi-objective optimal power flow considering transient stability based on parallel nsga-ii,” *IEEE Transactions on Power Systems*, vol. 30, no. 2, pp. 857–866, March 2015.

- [56] H. A. Mostafa, R. El-Shatshat, and M. M. A. Salama, “Multi-objective optimization for the operation of an electric distribution system with a large number of single phase solar generators,” *IEEE Transactions on Smart Grid*, vol. 4, no. 2, pp. 1038–1047, June 2013.
- [57] M. Patel, *Wind and Solar Power Systems*. Boca Raton,FL: CRC Press, 1999.
- [58] J. Seguro and T. Lambert, “Modern estimation of the parameters of the weibull wind speed distribution for wind energy analysis,” *Journal of Wind Engineering and Industrial Aerodynamics*, vol. 85, no. 1, pp. 75 – 84, 2000. [Online]. Available: <http://www.sciencedirect.com/science/article/pii/S0167610599001221>
- [59] S. Tewari, C. J. Geyer, and N. Mohan, “A statistical model for wind power forecast error and its application to the estimation of penalties in liberalized markets,” *IEEE Transactions on Power Systems*, vol. 26, no. 4, pp. 2031–2039, Nov 2011.
- [60] B. M. Hodge and M. Milligan, “Wind power forecasting error distributions over multiple timescales,” in *2011 IEEE Power and Energy Society General Meeting*, July 2011, pp. 1–8.
- [61] J. Wang, A. Botterud, R. Bessa, H. Keko, L. Carvalho, D. Issicaba, J. Sumaili, and V. Miranda, “Wind power forecasting uncertainty and unit commitment,” *Applied Energy*, vol. 88, no. 11, pp. 4014 – 4023, 2011. [Online]. Available: <http://www.sciencedirect.com/science/article/pii/S0306261911002339>
- [62] W. Ko, D. Hur, and J.-K. Park, “Correction of wind power forecasting by considering wind speed forecast error,” *Journal of International Council on Electrical Engineering*, vol. 5, no. 1, pp. 47–50, 2015.

- [63] S. Roy, "Market constrained optimal planning for wind energy conversion systems over multiple installation sites," *IEEE Transactions on Energy Conversion*, vol. 17, no. 1, pp. 124–129, Mar 2002.
- [64] J. M. S. Pinheiro, C. R. R. Dornellas, M. T. Schilling, A. C. G. Melo, and J. C. O. Mello, "Probing the new iee reliability test system (rts-96): HI-ii assessment," *IEEE Transactions on Power Systems*, vol. 13, no. 1, pp. 171–176, Feb 1998.
- [65] Y. M. Atwa, E. F. El-Saadany, M. M. A. Salama, and R. Seethapathy, "Optimal renewable resources mix for distribution system energy loss minimization," *IEEE Transactions on Power Systems*, vol. 25, no. 1, pp. 360–370, Feb 2010.
- [66] W. Kersting, "Radial distribution test feeders," in *Power Engineering Society Winter Meeting, 2001. IEEE*, vol. 2, 2001, pp. 908–912 vol.2.
- [67] R. C. Dugan, "Reference guide: The open distribution system simulator (openss)," Palo Alto, CA, USA, 2012.
- [68] "Matlab optimization toolbox," The MathWorks, Natick, MA, USA.
- [69] G. of Canada. (2017) Historical climate data. [Online]. Available: http://climate.weather.gc.ca/historical_data/search_historic_data.e.html
- [70] B. A. Robbins, H. Zhu, and A. D. Domnguez-Garca, "Optimal tap setting of voltage regulation transformers in unbalanced distribution systems," *IEEE Transactions on Power Systems*, vol. 31, no. 1, pp. 256–267, Jan 2016.
- [71] Y. Liu, J. Li, and L. Wu, "Coordinated optimal network reconfiguration and voltage regulator/der control for unbalanced distribution systems," *IEEE Transactions on Smart Grid*, pp. 1–1, 2018.

- [72] L. Gan and S. H. Low, “Chordal relaxation of opf for multiphase radial networks,” in *2014 IEEE International Symposium on Circuits and Systems (ISCAS)*, June 2014, pp. 1812–1815.
- [73] Y. Liu, J. Li, L. Wu, and T. Ortmeier, “Chordal relaxation based acopf for unbalanced distribution systems with ders and voltage regulation devices,” *IEEE Transactions on Power Systems*, vol. 33, no. 1, pp. 970–984, Jan 2018.
- [74] S. M. Frank and P. K. Sen, “Estimation of electricity consumption in commercial buildings,” in *2011 North American Power Symposium*, Aug 2011, pp. 1–7.
- [75] Y. M. Atwa, E. F. El-Saadany, M. M. A. Salama, and R. Seethapathy, “Optimal renewable resources mix for distribution system energy loss minimization,” *IEEE Transactions on Power Systems*, vol. 25, no. 1, pp. 360–370, Feb 2010.
- [76] <https://www.transnetbw.com/en/transparency/market-data/key-figures>.
- [77] J. Lofberg, “Yalmip : a toolbox for modeling and optimization in matlab,” in *2004 IEEE International Conference on Robotics and Automation (IEEE Cat. No.04CH37508)*, Sept 2004, pp. 284–289.
- [78] M. ApS, *The MOSEK optimization toolbox for MATLAB manual. Version 8.1.*, 2017. [Online]. Available: <http://docs.mosek.com/8.1/toolbox/index.html>